Comparative Evaluation of Computational Techniques For Estimating UAV Aerodynamic, Stability and Control Derivatives

A THESIS
SUBMITTED TO THE FACULTY OF THE GRADUATE SCHOOL
OF THE UNIVERSITY OF MINNESOTA
BY

Robert W. Ritchie

IN PARTIAL FULFILLMENT OF THE REQUIREMENTS
FOR THE DEGREE OF
MASTER OF SCIENCE

William Garrard, co-advisor
Demoz Gebre-Egziabher, co-advisor

May 2013

Acknowledgments

I would like to express my deepest appreciation to all those who provided me the possibility to complete this thesis. I would especially like to thank my advisers professors Gebre and Garrard. Professor Gebre taught the first controls course I took at the University and the way the subject was presented really got me excited to learn more. And Professor Garrard taught me so much about leadership and character, who would have guessed after our first presentation I would end up here. Thank you both for your time, comments, and encouragement through my time at the University. The department is lucky to have faculty of your caliber.

I would also like to thank all of my friends both in and out of school. Friends that were always there when problems needed solving, especially when deadlines got close. And friends to just hangout on the weekend. Having amazing people like you in my life is a great gift.

Finally none of this would be possible without my family. If there is one blessing in my life it is my family. The endless amount of encouragement and support you provide me can never be repaid. My sister Shelby and mother Valerie, two of the most beautiful and compassionate women I have ever met. And my father Bob, simply the man I have always wanted to be.

Dedication

This is dedicated to my grandfather, Howard Wayne Wright. A giant on who's shoulders I stand.

Abstract

The small UAV presents many advantages in size, cost, and portability. Because of this it is often desired to design many UAVs, one for each task, and often in a competitive environment. The designer needs a set of validated conceptual design tools that allow for rapid prediction of flight characteristics. The validation study will be conducted on the Ultra Stick 120 using a comparison of a Vortex Lattice method and Digital DATCOM to wind tunnel data. These computational tools are provided as a part of the CEASIOM software suite.

Contents

List of Figures

Nomenclature

Abbreviations and Acronyms

CAD	Computer aided design
CFD	Computational fluid dynamics
DATCOM	Data Compendium (US Air Force)
FASER	Free-flying Aircraft for Sub-scale Experimental Research
NASA	National Air and Space Agency
RMSE	Random mean square error
SSE	Sum of squares due to error
SSR	Sum of squares about the mean
UAV	Unmanned Aerial Vehicle

List of Symbols

α	Angle of attack
δ	Residual
Γ	Circulation
γ_0	Vortex strength
Ψ	Stream function
ρ	Air density
AR	Aspect ratio
c	Cord length
C_l	Coefficient of lift
C_{l0}	Coefficient of lift at 0 α
$C_{l\alpha}$	Lift curve slope
C_{lmax}	Maximum coefficient of lift
C_d	Coefficient of drag
C_{d0}	Minimum coefficient of drag
C_{di}	Induced drag coefficient
C_p	Coefficient of pressure
D	Drag
e	Efficiency factor
L	Lift
M	Mach number

m_0	Infinite wing lift slope
n	Number of data points
q	Dynamic pressure
R	Residual
R_{square}	Measure of residual
RE	Reynolds number
S	Main wing surface area
T	Thrust
t	Airfoil thickness
v	Velocity
v_∞	Free stream velocity
W	Weight
y	Response variable
$\hat{y}$	Predicted response
$\bar{y}$	Local mean

Chapter 1

Introduction

This thesis deals with the tools used for the design of Unmanned Aerial Vehicles (UAVs). The specific class of UAV considered are those of hobbyist R/C aircraft size, wing span under 8 feet. This size of UAV is of current significant interest because they are relatively cheap to produce and maintain. Also they can be flown in many areas larger craft would be prohibited.

UAVs of this size are being used in many emerging applications. For example the validation of guidance navigation and control software. Having access to a cheap and available test platform means the designers can test many iterations of their systems in a short period of time. Also there is less safety risk if for example a control law causes the aircraft to diverge.

While there is a large body of knowledge and tools developed for the design of manned aircraft, it is not clear whether these tools are applicable to the design of UAVs. In what follows we will discuss why this is the case and what the current state of the art is in tools for initial sizing of UAVs.

1.1 Initial Sizing

In order to lend context to the class of tools being used a discussion of initial sizing is presented.

The initial sizing phase is a search process to identify a set of design variables, which when coupled with appropriate modeling techniques, defines a vehicle that fulfills

its mission. Once this phase is over the design can be passed off to higher fidelity simulations to further refine the vehicle. Figure 1.1 illustrates the initial sizing phase and points out where carpet plots and CEASIOM (performance estimation software) are used.

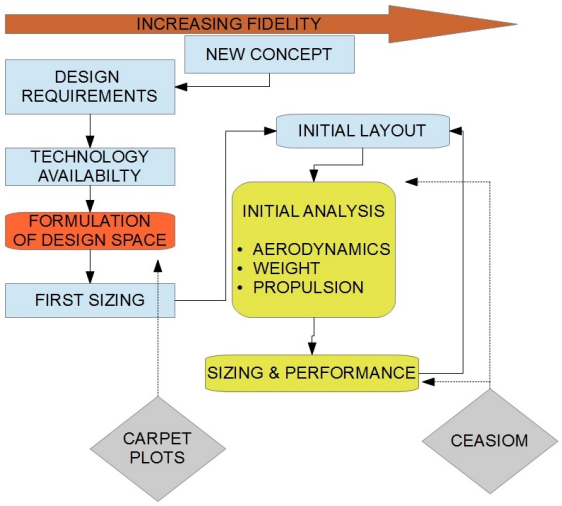

Figure 1.1: Overview of initial sizing process.

According to Raymer [1] there are six basic design variables.

- *T/W (used to size the engine as a ratio of weight)*
- *W/S (used to size the wing as a ratio of the weight)*
- *Aspect Ratio*
- *Taper Ratio*
- *Sweep*
- *Airfoil thickness/cord*

These are classic design variables based on years of aircraft design and can, in most cases, used directly in small UAV design. Certain considerations must be taken into account by the designer such as, often in small UAV design there are limited options of engines. Therefore T/W might not be appropriate for variation as the space is discreet and not continuous. These variables can be used to construct a carpet plot,

which is nothing more than a plot of the constrained design space based on mission objectives.

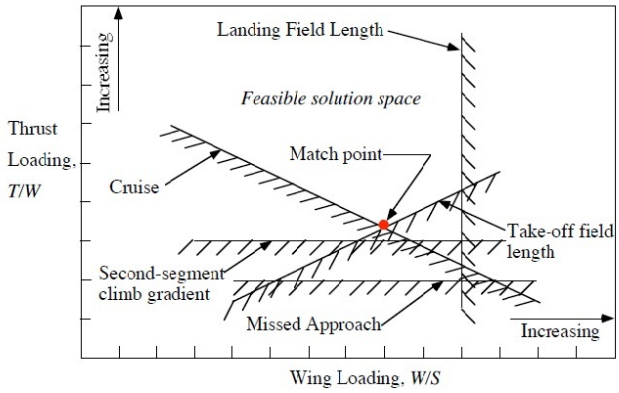

Figure 1.2: Demonstration of a carpet plot. from L.K. Loftin, Jr., "Subsonic Aircraft: Evolution and the Matching of Size to Performance," NASA RP 1060, Aug. 1980

These lines are created using simple Newton's second law relations. For example at cruise with thrust equal to drag the equality can be written as follows,

$$T/W = q\frac{C_{D_0}}{(W/S)_{cruise}} + \frac{(W/S)_{cruise}}{q\pi ARe} \tag{1.1}$$

and for stall speed, where $C_{l_{max}}$ is a function of C_{l_α} and α,

$$S/W = \frac{C_{l_{max}}}{.5\rho v_{stall}^2} \tag{1.2}$$

The carpet plot has said noting about whether or not the aircraft is actually buildable, just what the optimum point of the space is. This is where performance estimation techniques come in. Specifically these are used to estimate the parameters of the second law relationships. For example in Equation 1.1 an estimate of C_{D_0} is needed for a given proposed configuration.

Traditionally performance estimation has been broken down into three general phases of design. Initial design as previously discussed requires fast iteration and low cost. Then as the design progresses an increase of resources can be used in the process and more accurate techniques can be brought in. Figure 1.3 shows a basic overview of of this increasing accuracy in design process. The following sections will dive into

developing aircraft mathematical models, in other words estimating the performance of aircraft. Each method will be discussed with pros and cons presented.

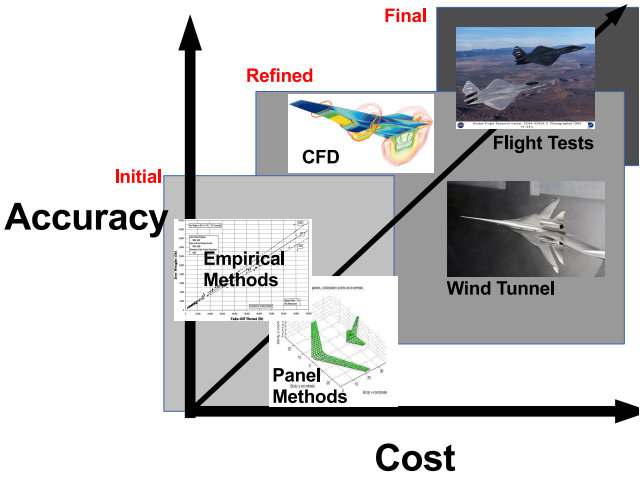

Figure 1.3: Separation of parameter estimation techniques by design phase. Also illustrating the relative cost and accuracy of the methods.

1.2 Developing Aircraft Mathematical Models

Aircraft model identification is accomplished by providing a mathematical description for the aerodynamics forces and moments in terms of flight conditions such as airspeed and orientation to the relative wind. Aerodynamic parameters and stability and control derivatives capture dependence of the forces and moments on the flight conditions. Methods have been developed to quantify these parameters these include, but are not limited to, wind tunnel testing, computational fluid dynamics, and empirical methods.

1.2.1 Wind Tunnel Testing Methods

Wind tunnel testing is the oldest of the methods. It involves placing a model of the aircraft on a force moment scale and controlling the flight conditions. With both of these known the parameters can be fitted. The most common type of wind tunnel can only perform static tests while special tunnels have be created that allow dynamics.

Special care must be taken in wind tunnel testing so that effects not associated with the forces and moments generated by the aircraft do not affect the measured quanti-

ties. There are many interference effects, for example blockage and deflection of the wind tunnel air stream, interference between the blades of the rotors, interference between appendages and lifting surfaces, between viscous wakes and nearby surfaces.

Also the flight conditions of the tunnel must accurately represent the flight conditions of the full aircraft. Otherwise no inference can be made about it's performance. This requires the matching of non dimensional parameters such as the Reynolds number and Prandtl number.

Wind tunnel testing remains the most accurate way of validating aircraft performance in off-design conditions. These are conditions where the computer codes have not been specialized or yet validated. Some examples are: simulation of complex shapes where grid generation poses a problem, simulation of separated flows, simulation of viscous effects in corners and gaps, and power effects. [2]

1.2.2 Computational Fluid Dynamics Methods

The progression of numerical methods for fluid mechanics involves solving increasingly accurate representations of the physical world. Over the last twenty years the focus has been on the solution of the Reynolds averaged Navier-Stokes (RANS)equations. These have proven to be the most accurate representation of the fluid flow physics. The software packages developed to solve these equations and their extensions have become very complex and involve flow simulation, CAD modeling, mesh generation, and post-processing.

Complex 3D shapes continue to pose the hardest challenge for CFD codes. As well as irregular, viscous, or separated flows. This is the area of simulation study that has been dominated by panel methods in the past. Even though the panel methods are often limited to non-viscous flows, they only require simple surface panels not 3D volume grids. The generation of the panels is highly automated versus the 3D volume grid that requires experience to ensure accuracy.

A hierarchy of codes is needed when doing CFD testing, much like specialized wind tunnels. There are large wind tunnel for power on effects, trans-sonic and sonic wind tunnels, and many others. In the same way CFD has codes specialized for separated flow, internal flows, and trans sonic / sonic flows just for example. Even when the accuracy of CFD cannot be guaranteed for some parameters CFD testing can still

play an important role . For example accurate drag calculations are still hard for even complex codes. But accurate lift simulations can be generated from many of the codes.

Even though CFD is becoming a mature tool it cannot be used in a black box sort of way. The user needs to understand the nature of CFD, its capabilities and also its pitfalls, in order to get useful simulation data. CFD is a tool and whether or not it is effectively used depends on the user. An example given in [3] "examining the pressure contours, the surface or field velocity vectors, etc. It is then possible to choose from an examination of inviscid surface pressures, streamline or velocity vector distributions, those that are less prone to flow separation, formation of strong shocks or favorable pitching moment characteristics, etc." [2] ends the discussion by stating "Experience is the key to success in such studies."

1.2.3 Approximate and Empirical Methods

In the early years of aircraft development aerodynamic parameters were estimated based on known performance data. Table of aircraft performance were generated and these tables would be used to predict the performance of the next design. These parameters came from first principle analysis of aircraft flight dynamics. Take for example the calculation of the lift curve slope of the fuselage wing combination. From [4] this is estimated to be

$$C_{L_{\alpha_{wf}}} = K_{wf} C_{L_{\alpha_w}} \tag{1.3}$$

where K_{wf} is the wing-fuselage interference factor found from,

$$K_{wf} = 1 + 0.025(\frac{d_f}{b}) - 0.25(\frac{d_f}{b})^2 \tag{1.4}$$

Equation 1.4 was produced by a line fit of a database of available aircraft configurations. These line fit methods proved very successful in the development of aircraft before the advent of modern computing. Consider the Concorde which first flew in 1969, a stable super sonic CFD code was not available until the year after 1970 [2].

The problem with these methods goes to the heart of small aircraft performance estimation, aerodynamic effects do not scale. Line fits of full size aircraft have little

validity at small scale. This is mainly attributed to the large different in Reynolds number effects or the ratio of inertial forces to viscous forces.

DATCOM [5] is one of these methods but is enhanced with the ability to do estimation of parameters using not only database fits but approximations from elliptical lift theory. It was created by the United States Air Force in conjunction with McDonnell Douglas Corporation in an effort to combine all the known estimation techniques with the low level computation techniques available like strip theory and elliptical lift theory. DATCOM will produce estimation results are very complete providing all of the stability derivatives as well as data for the creation of lift, drag, and pitching moment plots.

If fitting known data to assumed forms of aerodynamic models the next step in complexity is panel methods. These methods work by assuming the governing flow equations can be solved by the superposition of elementary flows. These elementary flows are sources, sinks, vortex ect. The lifting surfaces can be approximated with vortex flow while non-lifting surfaces can be approximated with sources and sinks. The use of the vortex for lifting surfaces allows for circulation which is a mathematical abstraction to describe a lifting flow field.

Panel methods can be used to estimate the full range of stability derivatives and performance. They are relatively easy to understand and many software packages are available that provide almost a black box experience. This is because they do not require an experienced user to create a 3D volume grid and often only require, for example, tuning the number of panels per wing.

1.3 Problem Statement

It is not clear if the approximate and empirical methods developed for sizing traditional manned aircraft can be applied to UAV performance prediction. In this class of aircraft often the designer does not have the time or resource to invest in high level CFD or wind tunnel database production. Its is certainly known that due to Reynolds number effects and scaling the results will not be as accurate. The accuracy of the results needs to be quantified such that if they are within the designers tolerance for error they can be used to guide the initial design of the UAV.

1.4 Thesis Contribution

This thesis will compare DATCOM and a vortex lattice code performance prediction of lift and drag to wind tunnel test results of a UAV. The amount of error between the predictions and the wind tunnel tests will be quantified and suggestions on error source will be made. So that the designer will know what to expect when attempting to use the codes for the initial design phase.

1.5 Thesis Organization

The remaining discussion will be broken down into three chapters. First the test bed aircraft will be described so that the reader can get a feel for the size of aircraft being discussed. Then the simulation methods will be described, both the theory and usage of the methods. Once the methods are described metrics will be created to quantify the results of the simulation in comparison to the wind tunnel results. Finally the metrics will be used to compare the results and the sources of error will be discussed.

Chapter 2

Benchmark Data

2.1 The FASER Platform

The aircraft used in this thesis is part of the FASER or Free-flying Aircraft for Sub-scale Experimental Research project [6]. Which was developed as an inexpensive sub-scale aircraft to conduct frequent testing of advanced dynamic modeling and control design. The project originated at NASA Langley Research Center (LaRC), which has a long history of sub-scale testing.

The aircraft itself was chosen to be relatively cheap with good aerobatic performance. The chosen aircraft is the Hanger 9 ARF Ultra-Stick 120 kit-built. The geometric characteristics of the airframe are listed in Table 2.1.

— **Fuselage** —	
Length	4.31 ft
Max. height	0.4167 ft
Max. width	0.3958 ft
— **Wing** —	
Reference area	8.28 ft^2
Span	6.29 ft
Mean geometric chord	1.42 ft
Leading edge sweep	0°
Aspect ratio	4.778
Taper ratio	1
Dihedral angle	0.7°
Twist	0°
Incidence at root	0°
—**Propeller**—	
Diameter	14.0 in
Pitch	9.5°
Number of blades (folding)	2

Table 2.1: Geometric characteristics of the FASER test bed aircraft.

Accurate models of the aircraft dynamics are needed for controls testing and design so the air frame needed to fit in an available wind tunnel. The tests where carried out in the NASA LaRC 12-foot Low-Speed Tunnel. Testing was completed to meet four objectives: to study the effects of power, to quantify the aerodynamic influence of the longitudinal location of the air data birds, to identify differences in power-on aerodynamics from the original FASER wind tunnel test to a new wind tunnel test, to investigate thrust and current draw of different size propellers. As a part of this testing high resolution power off α sweeps where conducted, these are used as the validation tests in this thesis. The full set of wind tunnel data is available on the University of Minnesota Digital Conservatory.

2.2 FASER Wind Tunnel and Flight Test Data

The wind tunnel testing was conducted on July 14-27, 2006 by Vanessa Aubchon, Bruce Ownes, Charlie Debro, and Wes O'Neal [7]. Specifically the data used in

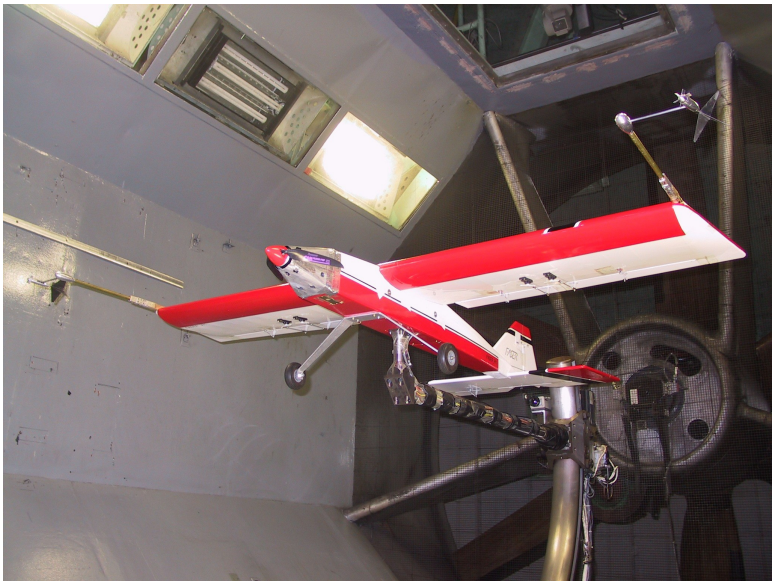

Figure 2.1: FASER mounted in the 12-Foot NASA LaRC Wind Tunnel.

this thesis can be found in runs 4,95,163,182 as these were determined to have the smoothest data points for curve fitting. The conditions of the tests are available in Table 2.2 and the location points of the data collection in Table 2.3.

Constant Parameters	
Dynamic Pressure	2 psf
S Reference	8.28 ft^2
b Reference	6.29 ft

Table 2.2: Constant values used in testing. Dynamic pressure was held constant throughout all tests.

Test	**α Measurements**	**Test Points**
4	-5,0,5,10,11.75,12.5,13.25,15,17.5,20,25,30,35,40	14
95	-5,0,5,10,11.75,12.5,13.25,15,17.5,20,25,30,35,40	14
163	-5:1:5, 5.5:0.5:10, 10.25:0.25:20, 20.5:0.5:25, 26:1:30, 32:2:40	81
182	-5:1:5, 5.5:0.5:10, 10.25:0.25:20, 20.5:0.5:25, 26:1:30, 32:2:40	81

Table 2.3: Alpha locations and number of data points of the tests used in analysis. Two low resolution α sweeps and two high.

The lift curve of the wind tunnel tests are presented in Figure 2.2.

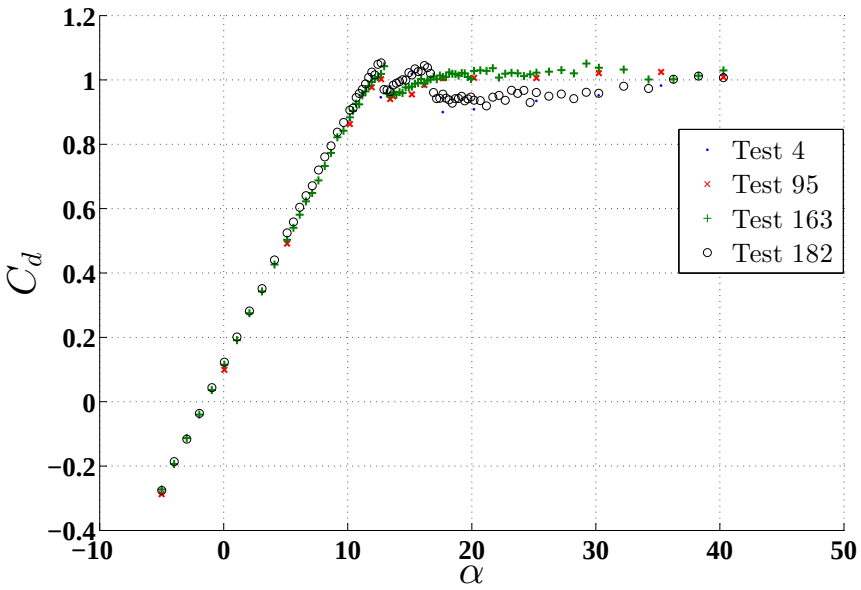

Figure 2.2: Lift curve for FASER wind tunnel tests.

The linear region of the lift curve is from $\alpha(-5)$ to $\alpha(11)$. After which FASER experiences the first stall. The fact that FASER experiences a first stall and then a second is still under discussion. A possibility presented in [6] is that the first stall is probably from laminar separation on the leading edge. While the second is a full wing stall from flow separation on the trailing edge progressing to the leading edge.

The drag polar of the tests is presented in Figure 2.3. Of note is how the drag polar increases rapidly in the stall region of $C_l \approx 1$.

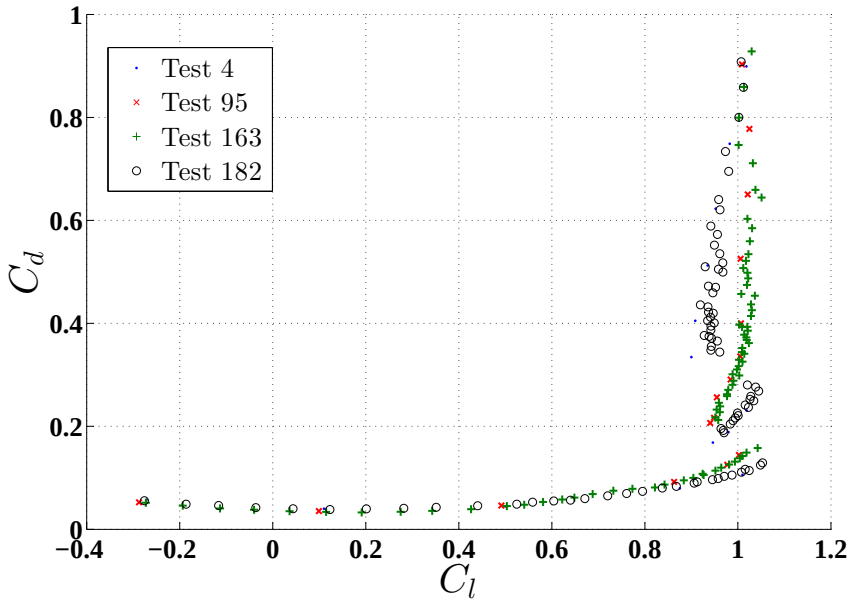

Figure 2.3: Drag Polar for FASER wind tunnel tests.

Chapter 3

Methods and Usage

3.1 Digital DATCOM

The United States Air Force Digital DATCOM is a FORTRAN implementation of the United States Air Force DATCOM document and is used to estimate aircraft performance. The program to digitize DATCOM was started in 1976 in an effort to automate the methods contained in the DATCOM document. Although there have been updates much of the core remains the same. DATCOM is a semi empirical method that uses look up tables to calculate certain aspects of aircraft performance. These were populated by years of wind tunnel testing. The DATCOM manual [5] says users have the option of substituting certain experimental data to be used in lieu of the contained data. The example provided, in the manual, is in the body wing interaction calculations as these are often hard to calculate. In addition to empirical methods DATCOM has direct calculation methods that can be combined with empirical data. For example transforming the flow around a sphere into that around the airfoil, then an empirical viscous method from Kinsy and Bowers is used to correct for viscous effects [5]. In this way empirical methods can be combined with aerodynamic models in an attempt to produce the most accurate results.

To illustrate how DATCOM combines lifting line and other theories with empirical data the following example is taken from the DATCOM manual. The DATCOM method to calculate the section lift-curve slope (c_{l_α}) is,

$$c_{l_\alpha} = \frac{1.05}{\beta}[\frac{c_{l_\alpha}}{(c_{l_\alpha})_{theory})}](c_{l_\alpha})_{theory} \tag{3.1}$$

where $[\frac{c_{l_\alpha}}{(c_{l_\alpha})_{theory})}]$ is an empirical correction factor. This factor accounts for the development of the boundry layer towards the airfoil trailing edge. $(c_{l_\alpha})_{theory}$ is the theoretical airfoil lift-curve slope from the Kutta Joukowki hypothesis. Which is the theorem that can be used to related the 2D flow around a cylinder to the generated lift of one unit of span. β is the Prandtl-Glauert compressibility correction factor $\sqrt{1-M^2}$. Finally the constant 1.05 is an empirical correlation factor based on a large test data base of the function. Because DATCOM uses these types of methods

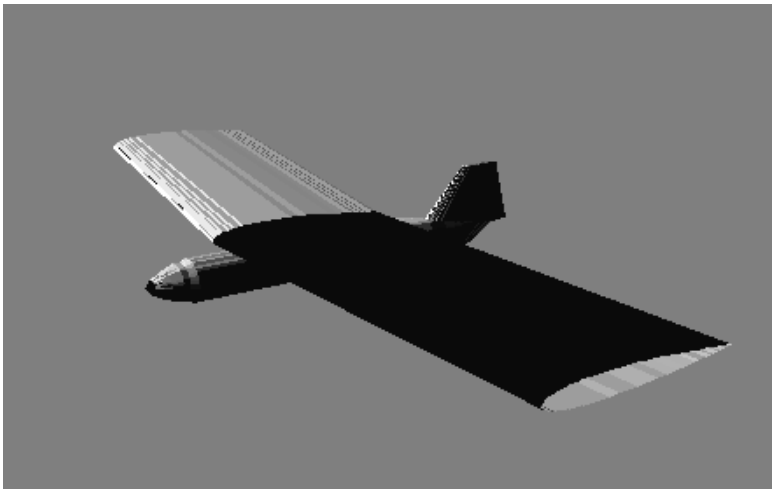

Figure 3.1: Visual representation of FASER in the DATCOM input file. Representation is only an approximation of the input file.

it has input limitations. The shape of the body segments are restricted as follows: nose and tail shapes must be either an oblate or conical, after bodies must be cylindrical while tails may be either boat-tailed or flared. According to the manual the main concern for the small UAV designer is "users are advised to be mindful of section characteristics which are sensitive to Reynolds number, particularly in cases where very low Reynolds number estimates are of interest". A typical example would be pretest estimates for small, laminar flow wind tunnels where Reynolds numbers on the order of 100,000 are common. Users should be aware that the Datcom and Digital Datcom employ turbulent skin friction methods in the computation of friction drag values. Estimates for cases involving significant wetted areas in laminar flow will require adjustment by the user. [5]

3.2 Vortex Lattice

The main assumption of panel methods are incompressible, irrotational flow, referred to as potential flow [8]. By assuming potential flow the governing fluid motion equations are simplified. By substituting potential flow into the continuity equation,

$$\frac{\partial p}{\partial t} + u\frac{\partial p}{\partial x} + p(\frac{\partial u}{\partial x} + \frac{\partial v}{\partial y}) = 0 \tag{3.2}$$

the solution can be written as a 2D version of the Laplace equation,

$$\frac{\partial^2 \Phi}{\partial x^2} + \frac{\partial^2 \Phi}{\partial y^2} = 0 \tag{3.3}$$

The principle of superposition can be used to find a solution to the Laplace equation in terms of the superposition of elementary flows along a stream line. The vortex panel method utilizes the elementary solution to vortex flow and uniform flow along a streamline. The stream function of vortex low is,

$$\Psi = \frac{\Gamma}{2\pi}\ln(r) \tag{3.4}$$

The vortex solution is singular, and therefore, vortex lattice codes use vortices of infinitesimal strength. Thus Equation 3.4 is rewritten using this and polar coordinates as,

$$\oint \frac{\gamma_0}{2\pi}\ln(|r - r_0|)ds_0 \tag{3.5}$$

The integral is evaluated over all the vortex elements on the airfoil surface. To add uniform flow the stream functions are added using superposition.

$$\Psi = V_\infty y \tag{3.6}$$

$$\Psi = u_\infty y - v_\infty x - \oint \frac{\gamma_0}{2\pi}\ln(|r - r_0|)ds_0 \tag{3.7}$$

Panel methods are evaluated only at the streamline on the surface of the airfoil because the body surface is considered a streamline. This stream line will just be some constant C. Thus Equation 3.7 is written as

$$\Psi = u_\infty y - v_\infty x - \oint \frac{\gamma_0}{2\pi} \ln(|r - r_0|) ds_0 - C = 0 \tag{3.8}$$

over all points on the surface of the airfoil. Equation 3.8 can be discretized and evaluated numerically over the individual panels. At each point on the surface of the airfoil the coefficient of pressure C_p, vortex strength, and potential flow velocity can be related by

$$C_p = 1 - \frac{\gamma_0^2}{V_\infty^2} \tag{3.9}$$

Thus the pressure distribution can be used in post processing to determine the lift and pitching moments. In order to determine drag the vortex lattice method must be combined with boundary layer analysis or other methods.

The specific vortex lattice implementation included in CEASIOM is Tornado [9] which has been further updated by the CEASIOM team. TORNADO allows a user to define most types of contemporary aircraft designs with multiple wings, both cranked and twisted with multiple control surfaces located at the trailing edge. Each wing is permitted to have unique definitions of both camber and chord. The TORNADO solver computes forces, moments, and the associated aerodynamic coefficients. The aerodynamic derivatives can be calculated with respect to: angle of attack, angle of sideslip, roll-pitch-yaw rotations, and control surface deflections.

Tornado is based on standard vortex lattice theory, previously discussed. In Tornado the wake coming off the trailing edge of every lifting surface is flexible and changes shape according to the flight condition. For example: a rolling aircraft will have a "corkscrew" shaped wake, which will influence the aerodynamic coefficients. The classical "horse-shoe" arrangement of other vortex-lattice programs has been replaced with a "vortex-sling arrangement. It basically works in the same way as the "horse-shoe procedure with the exception that the legs of the shoe are flexible and consist of seven (instead of three) vortices of equal strength. One of the primary assumptions in the vortex lattice theory is the small angle of attack. Therefore, caution is advised

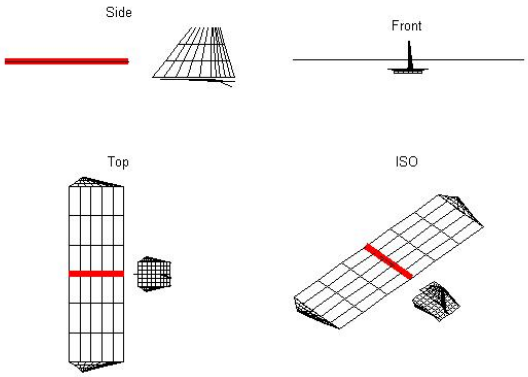

(a) Panels of Ultra Stick 120 in TORNADO

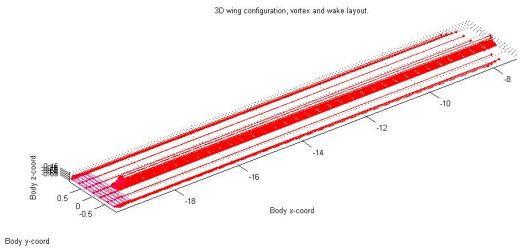

(b) Ultra Stick 120 wake in TORNADO

Figure 3.2: Graphical representation of Ultra Stick 120 in TORNADO

when examining large angles as well as large rotational speeds. Compressibility effects are neglected, as are thickness effects of the lifting surfaces. In TORNADO, every flat surface is considered as a wing, this means that there are no differences in input or calculation between main wing, stabilizer or fin. [9]

To account for viscous effects, CEASIOM provides a correction to the steady vortex lattice method by the strip theory that combines the linear potential results with the 2D viscous airfoil code XFOIL. [10] XFOIL is able to calculate a compressibility correction with the Karmen-Tsien method. As well as boundary layer analysis such as forced or free transition and separation.

3.3 CEASIOM and Usage

Now that the methods have been chosen and discussed an implementation of the methods is needed. CEASIOM is a software wrapper around the simulations that provides many nice features. It will be discussed in the following section.

3.3.1 Intro

The CEASIOM software package was created as a part of the SimSAC Project and stands for the Computerized environment for Aircraft Synthesis and Integrated Optimization Methods. It is a multidisciplinary tool focused on the conceptual design and analysis of fixed-wing aircraft. Some of the included disciples are aerodynamics, structures, and flight dynamics. Which all have major impacts on an aircraft performance. It aims to provide access to higher fidelity tools than textbook methods while still retaining the ease of calculation and rapid iteration of design. CEASIOM is able to take information from all of these sources and produce detailed aerodynamic tables as well as input the data into a six degree of freedom flight simulator. As of writing CEASIOM could be obtained at *www.ceasiom.com* along with many tutorials related to its use on full scale aircraft. The discussion to follow will therefore be concerned with the specific challenges in using the software for UAV design.

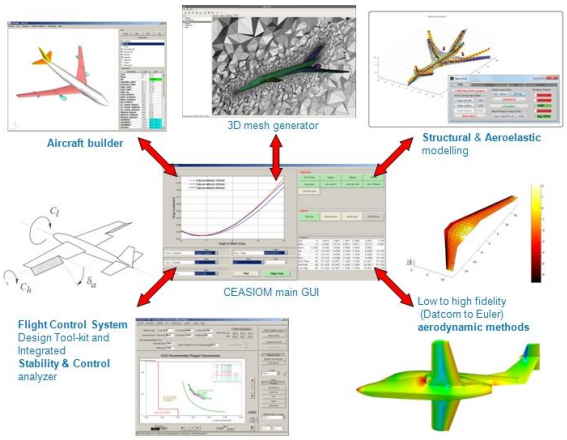

Figure 3.3: A graphical description of the CEASIOM work flow

3.3.2 ACBuilder

ACBuilder is the entry point of the application for a new design. ACBuilder is a simplified CAD system that defines aircraft with a minimal number of parameters.

The system can take this simple input and covert it to the geometric tables needed for the input into the aerodynamic module. This is a standardized file definition that was also developed by the SimSAC Project to be a standard across conceptual design tools. It is stored as geo.xml in the home directory of the project. The minimal parameter definition scheme that ACBuilder uses works great for man sized aircraft but the geometric calculations done to create geo.xml with these parameters can lead to bugs in the definition file. The data is stored in tree structured xml form. A visual example of the tree network can be seen in figure 3.4.

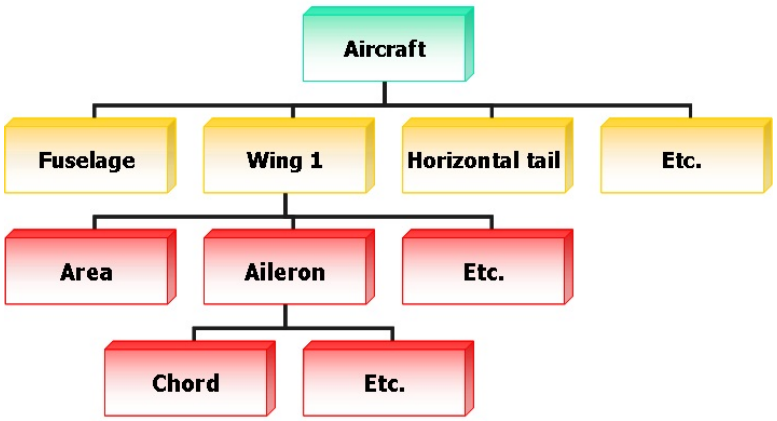

Figure 3.4: Ceasiom geo.xml data storage scheme

The limitations on the Vortex Lattice and DATCOM methods are present in ACBuilder, for example there is no option to model the undercarriage. The fuselage is a body of revolution and is modeled according to figure 3.5,

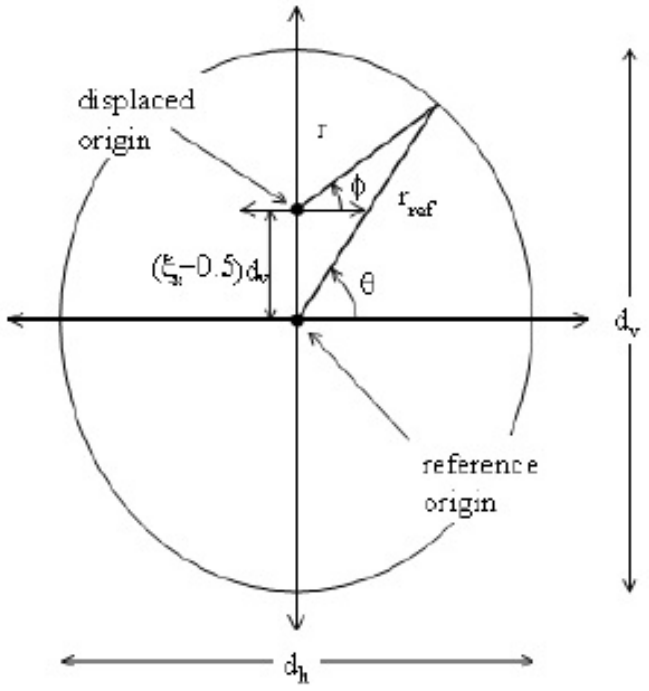

Figure 3.5: ACBuilder body definition

In order to avoid the current bugs it was found that starting a small UAV from the X-31 starting point yielded the most stable geometric definition.

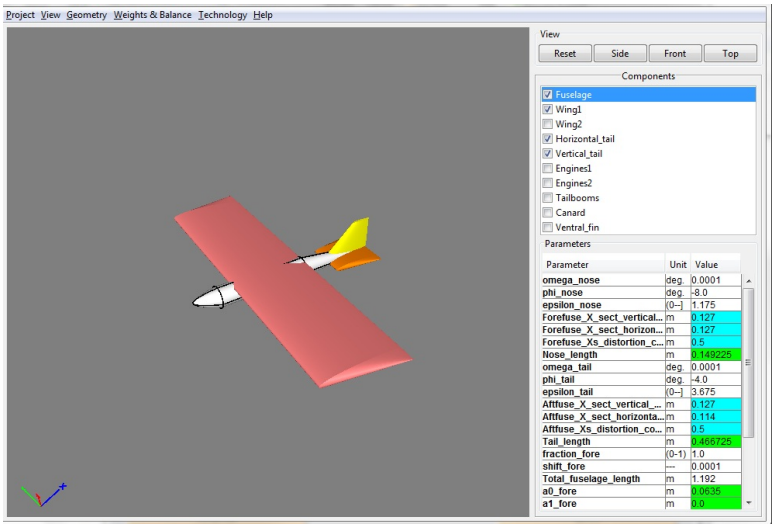

Figure 3.6: Ultra 120 in ACBuilder

3.3.3 Weights and Balance

The Weights and Balance module will take input from the geo.xml file and estimate the moments of inertia of the aircraft. Another one of the problems with the current version of ACBuilder is that it expects at least one pilot and will attempt to include the pilots weight in the weight and balance calculations. It was found that by using the Raymer method this fact can be ignored and values similar to those obtained through experiment can be achieved. Another option is to allow the Weight and Balance module to write to the geo.xml file and then edit the xml by hand and input experimental inertial data.

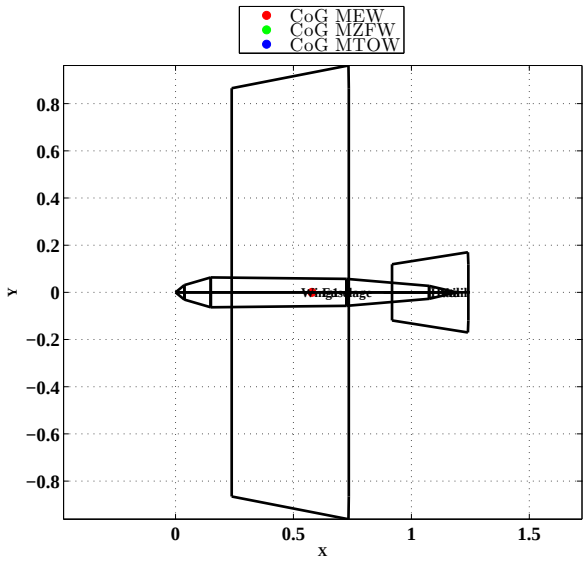

Figure 3.7: Ultra 120 in Weights and Balance

Figure 3.7 shows the location of of the CG point from the Raymer method. Only the location of the maximum empty weight is shown as the bug requiring at least one pilot throws off the take off weight and landing weight. Again

3.3.4 Aerodynamic Model Builder

This is the final module used to translate between the geometric definition determined by CEASIOM to the input geometry of the solvers. This is a great asset to the designer and is what gives the solvers almost black box usage. The green boxes in the upper

right of Figure 3.8 show the eight steps to initialize and run the simulations.

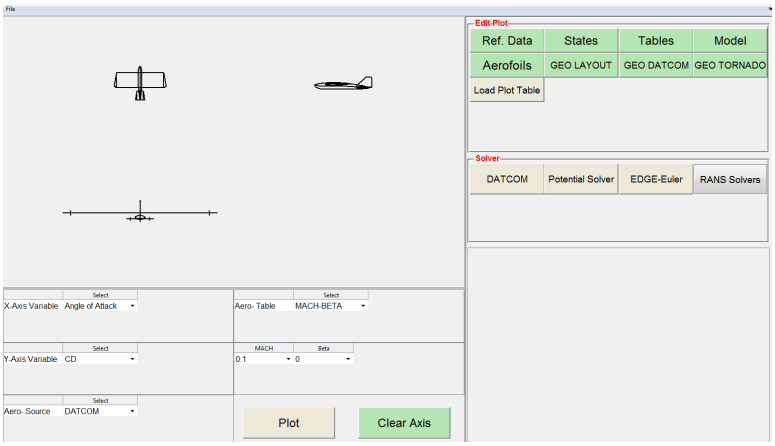

Figure 3.8: Ultra 120 in AMB

The first five steps pertain to the loading of the generated CEASIOM files in the previous modules. Here the designer can specify the states of the simulation. Then the last three steps tell AMB which solver you want the data translated to and once everything is loaded and correct all buttons should be green. All that remains for the user is to click run on the appropriate solver and extract the data.

Chapter 4

Quantifying the Performance of Approximate and Empirical Methods

In this chapter the mathematical models generated by DATCOM and Vortex Lattice methods will be compared against the wind tunnel test data. First the metrics used for assessing the quality of DATCOM and Vortex Lattice will be discussed. Then the metrics will be used to compare the models ability to correctly predict the lift and drag characteristics of a UAV.

4.1 Parameters for Comparison

For comparison, parameters related to the lift and drag of the aircraft are chosen. These are the non-dimensional values of the lift coefficient C_l and drag coefficient. The coefficients will be calculated based on the total wing area,

$$C_l = \frac{L}{1/2\rho v^2 S} \tag{4.1}$$

$$C_d = \frac{D}{1/2\rho v^2 S} \tag{4.2}$$

The coefficient of lift is a function of angle of attack $C_l \equiv f(\alpha)$ and the plot of C_l

versus α is referred to as the lift curve. A sample lift slope can be seen in figure 4.1.

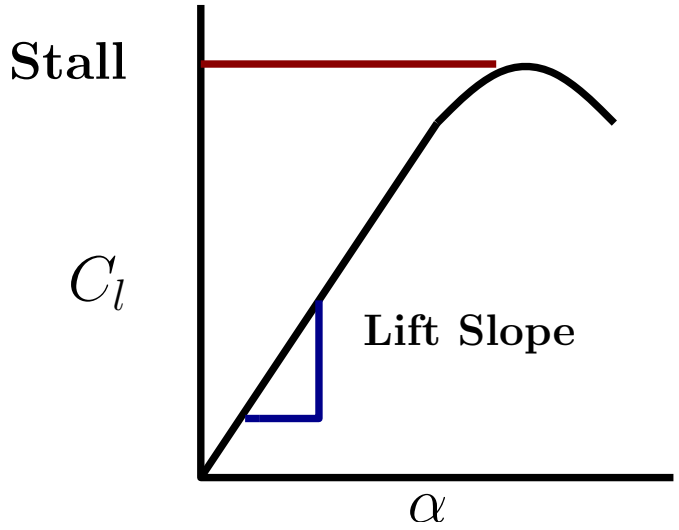

Figure 4.1: Sample lift curve showing parameters C_{l0} and $dC_l/d\alpha$

The parameters related to lift are C_{l0}, the lift produced at zero angle of attack, and $dC_l/d\alpha$ or the slope of the linear portion of the lift curve. We will assume the C_l vs α curve can be written as a linear function given by

$$C_l = C_{l_0} + C_{l_\alpha}\alpha + \mathcal{O}(t^n) \tag{4.3}$$

Where the higher order terms ($\mathcal{O}(t^n)$) are small. This means the fit in the comparison regions will provide the parameters of the region as shown in the following equation,

$$C_l = K_0 + K_1\alpha \tag{4.4}$$

Similarly the coefficient of drag is a function of α and therefore a change of variables to make it a function of C_l is possible, $C_d \equiv f(C_l)$. The plot of C_l vs. C_d is referred to as the drag polar. The change of variables and the plot of the drag polar give more physical meaning to the parameters associated with drag. Figure 4.2 shows a typical drag polar. Classically drag is broken down into a two term equation, shown in Equation 4.5.

$$C_d = C_{d0} + C_{di} \tag{4.5}$$

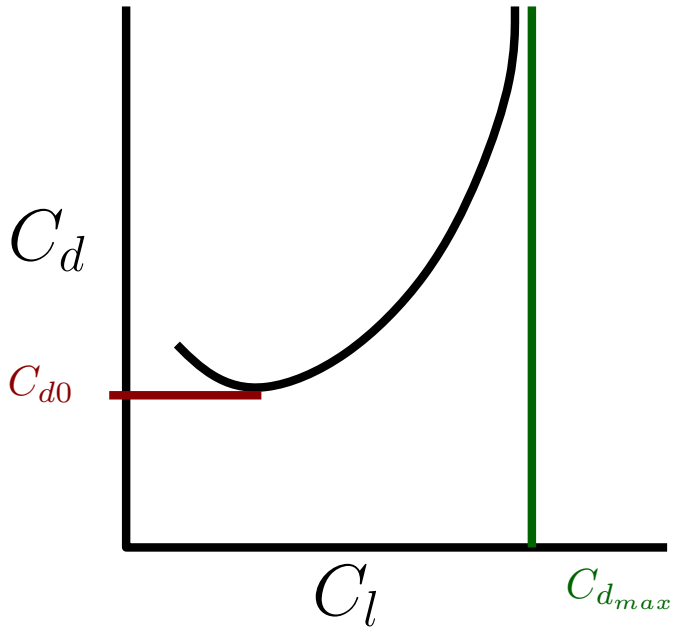

Figure 4.2: Sample drag polar

Where C_{d0} is the zero lift drag, C_{di} is the induced drag. Both terms lump many different sources of drag. Zero lift drag is the sources not associated with the generation of lift and conversely C_{di} is a consequence of lift generation. From analysis of elliptic lift a more practical equation 4.5 can be written

$$C_d = C_{d0} + \frac{C_l^2}{\pi e A R} \tag{4.6}$$

A more accurate model for curve fitting can be written as Equation 4.7 where a term proportional to C_l is included. This can be thought of a loosely related to the pressure drag and is often negative acting in the opposite direction of the drag axis.

$$C_d = K_0 + K_1 C_l + K_2 C_l^2 \tag{4.7}$$

The parameters K_0 K_1 K_2 can then be related back to the form drag and induced drag concept. But in regions where the minimum point of the drag polar is not contained the parameters are just curve fit parameters and can loosely be interpreted based on their relation to C_l.

In order to determine the coefficients a least squares method is chosen. Specifically

the method minimizes the sum of squares of the vertical deviations,

$$R^2 = \sum [y_i - f(x_i, a_1, a_2, \ldots, a_n)]^2 \tag{4.8}$$

Equation 4.8 can be solved efficiently in matrix form as,

$$b = (X^T X)^{-1} X^T y \tag{4.9}$$

where b is a vector of the coefficients and X is the input matrix and y is the output.

4.2 Comparison Metrics

The comparison metrics will be broken down into three steps. First a residual plot will be created for visualization of the error. Then the line will be fit according to the models of Equations 4.3 and 4.7. One line fit will be fit in the least squares method to the four wind tunnel test runs. Then the individual parameters residuals from the fit will be computed as

$$\Delta = \frac{P_{windtunnel} - P_{simulation}}{P_{windtunnel}} \tag{4.10}$$

Where $P_{windtunnel}$ is the parameter calculated by fitting the wind tunnel data and is used to normalize the parameters fit to the simulation results.Finally the goodness of the fits will be quantified by the following metrics.

Sum of squares due to error or SSE is used to measure the total deviation of the experimental values from the fit to these values. This is also known as the summed square of residuals. Note, in the goodness of fit equations y is the response, $\hat{y}$ is the predicted response, or curve location, and $\bar{y}$ is the local mean value.

$$SSE = \sum_{i=1}^{n} (y_i - \hat{y}_i)^2 \tag{4.11}$$

Values closer to zero indicate the fit is closer to the values of the experiment.

R-Square is a measure of how well the fit explains the variation in the data. In this

way it is the square of the correlation between the experimental values and the fit. R-square is defined as the ratio of the sum of squares of the regression (SSR) and the total sum of squares (SST). SSR is defined as

$$SSR = \sum_{i=1}^{n} (\hat{y}_i - \overline{y_i})^2 \tag{4.12}$$

SST is also called the sum of squares about the mean, and is defined as

$$SST = \sum_{i=1}^{n} (y_i - \overline{y_i})^2 \tag{4.13}$$

where SST = SSR + SSE. Given these definitions, R-square is given as

$$R_{square} = \frac{SSR}{SST} \tag{4.14}$$

R-square will be a value from 0 to 1, with a value closer to 1 meaning a greater amount of the variance is accounted for in the fit. The value is directly related to the percentage of the total variation explained.

Finally the root mean squared error is also known as the fit standard error and the standard error of the regression. It is an estimate of the standard deviation of the random component in the data, and is defined as

$$RMSE = s = \sqrt{MSE} \tag{4.15}$$

where MSE is the mean square error or the residual mean square and is given by,

$$MSE = \frac{1}{n} \sum_{i=1}^{n} (\hat{y}_i - y_i)^2 \tag{4.16}$$

4.3 Flight Regions for Comparison

The flight regions will be broken down by angle of attack. For the drag polar the C_l region will be determined from the lift curve. The three regions are presented in the following table.

Small angle of attack	$0 \leq \alpha \leq 5$
Medium angle of attack	$5 \leq \alpha \leq 10$
High angle of attack	$10 \leq \alpha \leq 15$

Table 4.1: Three regions of comparison to be used based on angle of attack

4.4 Wind Tunnel Results

The data from the wind tunnel tests discussed in Section 4.3 will first be analyzed in the linear region of the lift curve then separated by the three regions. By looking at the linear region of the wind tunnel data the overall parameters can be matched for FASER. The fits of the lift curve and drag polar will be split by sub section. This is not to say they are decoupled but for organization. This organization will be carried over to the discussion of the simulation results.

4.4.1 Linear Region

4.4.1.1 Lift Curve

The first thing to check when doing parameter matching is the goodness of fits. If the fits are not good the model being fit is incorrect. The lift curve goodness of fit for the linear region can be found in Table 4.2 and per the previous discussion are good.

SSE	0.01283
R-Squared	0.9988
RMSE	0.01416

Table 4.2: Goodness of fit metrics of the lift curve fit of the wind tunnel results in the linear region

Figure 4.3 shows the fit of the lift curve and the 95% confidence bounds. The parameters generated by the fit are presented in Table 4.3.

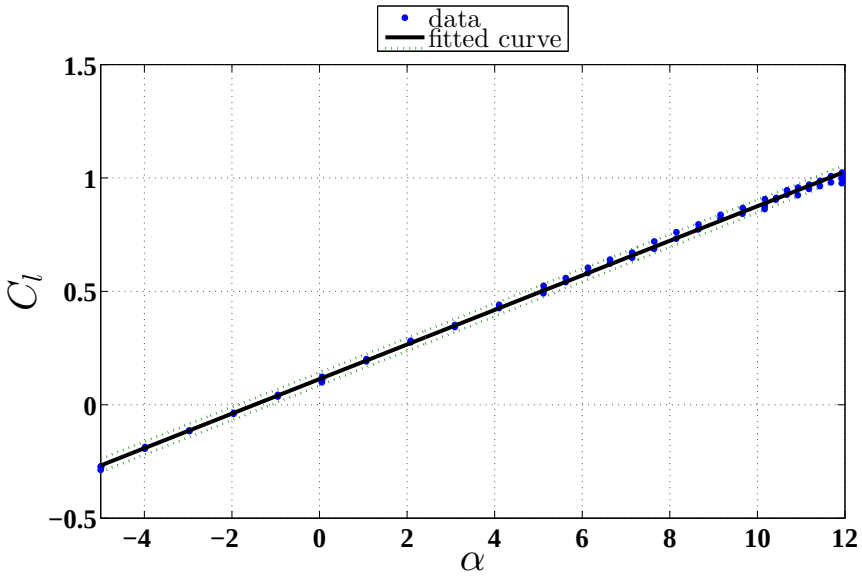

Figure 4.3: Linear fit of lift curve for the wind tunnel data linear region. The dotted lines denote the 95% confidence bounds.

K_0	0.1134
K_1	0.0762

Table 4.3: Matched parameters of the lift curve fit.

The value of these parameters yield the first interesting result that will be brought up extensively throughout the remaining discussion. Because the two methods in question use potential flow assumptions elliptical lift and thin airfoil theory can be used as a comparison to see what would be the expected errors. From the matched parameters two specific results from thin airfoil theory for symmetric airfoils are violated. First, the sectional lift coefficient is directly proportional to the angle of attack, thus it should be zero at zero α. Second, the lift sectional curve slope m_0 equals 2π per radian or about .1097 per degree. The lift slope is corrected using the elliptical finite wing correction,

$$C_{l_\alpha} = \frac{m_0}{1 + m_0/\pi AR} \tag{4.17}$$

to yield $C_{l_\alpha} \approx .10889$. Comparing this to the results in Table 4.3 it is expected then

that the simulations will produce curves shifted by the error at zero α which would result in parallel lines. But it is also expected that the unmodeled geometry will also have an impact on the slope. This is because the fuselage and other unmodeled parts are actually lifting surfaces and contribute to both the zero value and the slope.

4.4.1.2 Drag Polar

The goodness of fit metrics for the drag polar in Table 4.4 show good agreement that the fitted model matched the data set. Which can be seen in Figure 4.4

SSE	0.002241
R-Squared	0.9579
RMSE	0.005964

Table 4.4: Goodness of fit

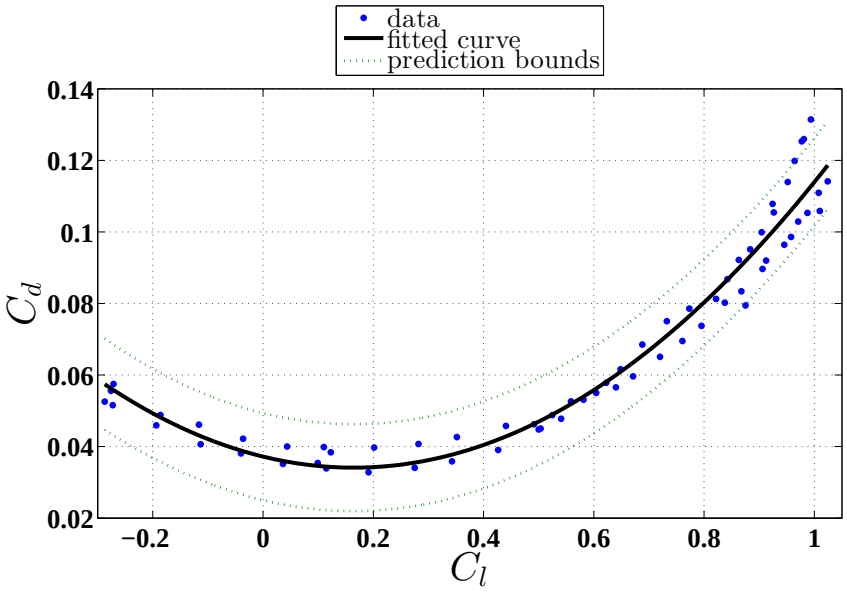

Figure 4.4: Quadratic fit of drag polar and residuals

K_0	0.0372
K_1	-0.0376
K_2	0.1143

Table 4.5: Parameters

A similar thin airfoil elliptic lift discussion can be made about the drag polar. Assuming $e = 1$ in Equation 4.6 C_{di} can be approximated by,

$$C_{di} = \frac{C_l^2}{AR\pi} \tag{4.18}$$

This approximation can be used as a lower limit for the drag polar. This sets $K_2 = 1/4.778\pi$ or $K_2 \approx .06366$. Table 4.5 shows a lower value of K_2. For the uncorrected vortex lattice it is expected that this value will be the lower limit on K_2 and the other two parameters will be zero as it is only predicting induced drag. The other two simulations attempt to calculate viscous forces and DATCOM will take the body into account. But as

4.4.2 Region I

4.4.2.1 Lift Curve

The lift curve goodness of fit for Region I can be found in Table 4.6 and per the previous discussion are good.

SSE	0.001307
R-Squared	0.9965
RMSE	0.009661

Table 4.6: Goodness of fit metrics of the lift curve fit of the wind tunnel results $0 \leqslant \alpha \leqslant 5$ degrees.

Figure 4.5 shows the fit of the lift curve and the 95% confidence bounds. The parameters generated by the fit are presented in Table 4.7.

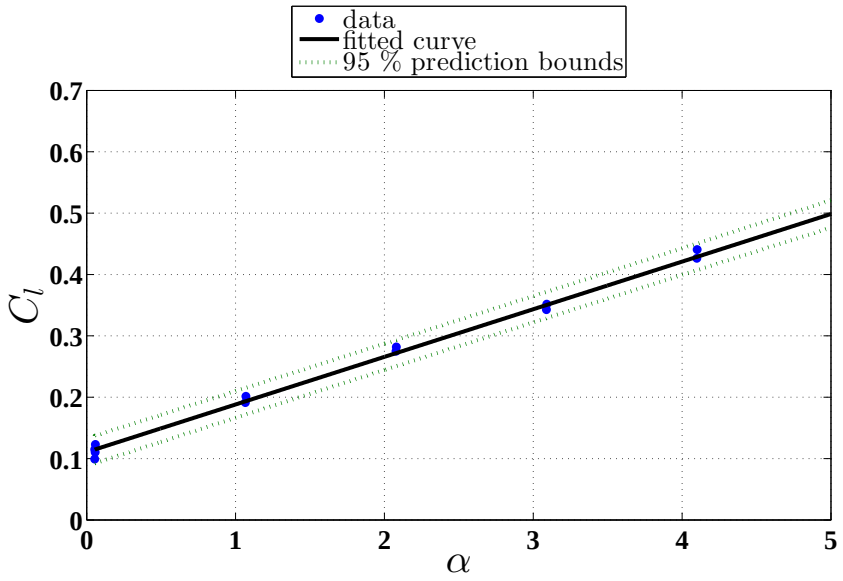

Figure 4.5: Linear fit of lift curve for the wind tunnel data $0 \leqslant \alpha \leqslant 5$ degrees. The dotted lines denote the 95% confidence bounds.

K_0	0.1105
K_1	0.07762

Table 4.7: Matched parameters of the lift curve fit.

The parameters in this region are nearly identical to the linear region as 0 α is included in the region. They will differ slightly due to the fitting of a smaller data set.

4.4.2.2 Drag Polar

The goodness of fit metrics for the drag polar in Table 4.8 show why having just one measure of goodness is not advisable. The R-Squared metric is not as good as in the lift curve. Inspecting Figure 4.6 visually shows this is because none of the data points lay on the fitted line. But the fitted line does appear to lay in a reasonable middle ground between the data points. The other two statistics are good this is because the line appears to traverse the middle of the data set.

SSE	0.0001122
R-Squared	0.6968
RMSE	0.002938

Table 4.8: Goodness of fit

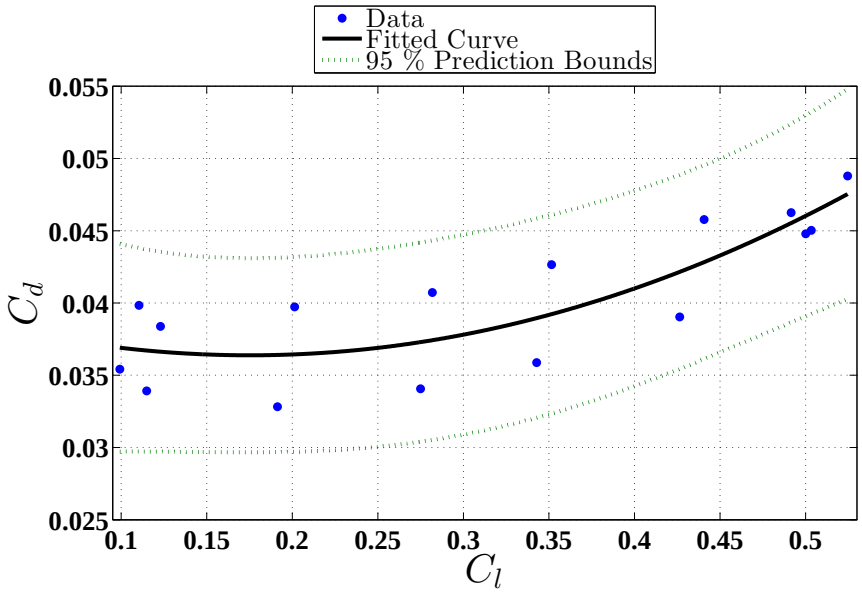

Figure 4.6: Quadratic fit of drag polar and residuals

K_0	0.09132
K_1	-0.03197
K_2	0.03918

Table 4.9: Parameters

As discussed earlier breaking down the region causes the parameters to loose their classical physical interpretations, but provide a way to judge the performance in a zoomed in sense. This can be seen in the results of this region. The influence of the form drag can be seen in the increasing of K_0 and the decreasing of the lift dependent parameters, K_1 and K_2. Its expected that the codes predicting form drag will also reflect this.

4.4.3 Region II

Looking at table 4.10 the goodness of fits are good.

4.4.3.1 Lift Curve

SSE	0.005202
R-Squared	0.9889
RMSE	0.01472

Table 4.10: Goodness of fit

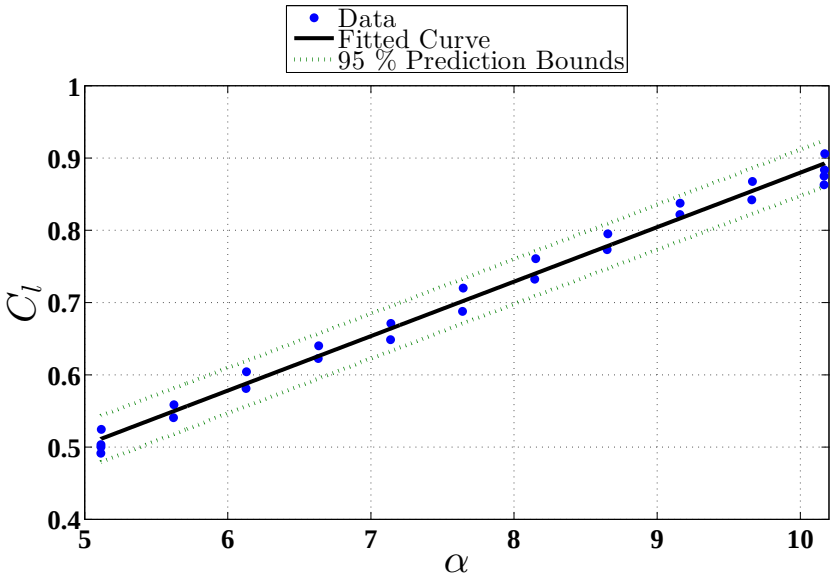

Figure 4.7: Linear fit of lift curve

		95% confidence bounds
K_0	0.1257	(0.09935, 0.1521)
K_1	0.07541	(0.07205, 0.07877)

Table 4.11: Parameters

The parameters are getting farther from the ideal elliptic lift prediction. This is most likely due to the un-modeled geometry and now that K_1 is changing this may be

an effect of a slight dependence on α^2 or the higher order terms. In other words in this region the lift performance,compared to ideal, is even worse due to an increased production of lift.

4.4.3.2 Drag Polar

The goodness of fit for the drag polar in this region has a better R-Squared value than Region I. This can be seen by looking at Figure 4.8. The data points are closer to the fitted line. While the other two metrics are still similar to the metrics of Region I.

SSE	0.0003037
R-Squared	0.9519
RMSE	0.003634

Table 4.12: Goodness of fit

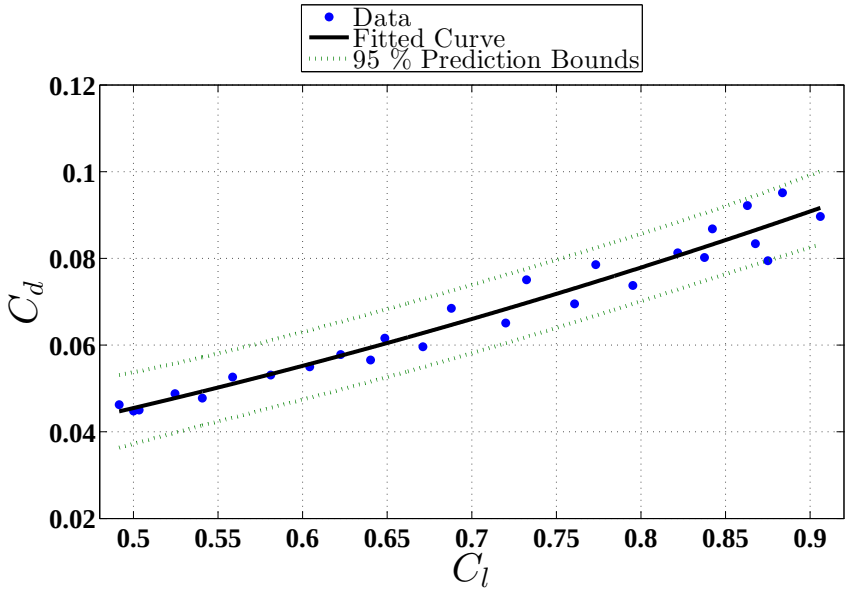

Figure 4.8: Quadratic fit of drag polar and residuals

		95% confidence bounds
K_0	0.05354	(-0.0498, 0.1569)
K_1	0.03842	(-0.106, 0.1828)
K_2	0.05354	(-0.0498, 0.1569)

Table 4.13: Parameters

The K_2 term is getting closer to the ideal lift prediction. The contribution of the fuselage and extra geometry can be seen in the increase and sign flip of K_1. Drag proportional to C_l has increased so much that the pressure drag contribution opposite to the drag axis is being overtaken.

4.4.4 Region III

4.4.4.1 Lift Curve

In this region stall sets in and the fits are no longer reliable. SSE and RMSE are ten times worse than Region II and R-Squared shows a large distribution of points. This can be seen visually in Figure 4.9 with points lying outside of the 95% confidence interval. The parameters in this region cannot be trusted for physical interpretation and will just be used to compare to the stall prediction of the simulations.

SSE	0.06689
R-Squared	0.2677
RMSE	0.03657

Table 4.14: Goodness of fit

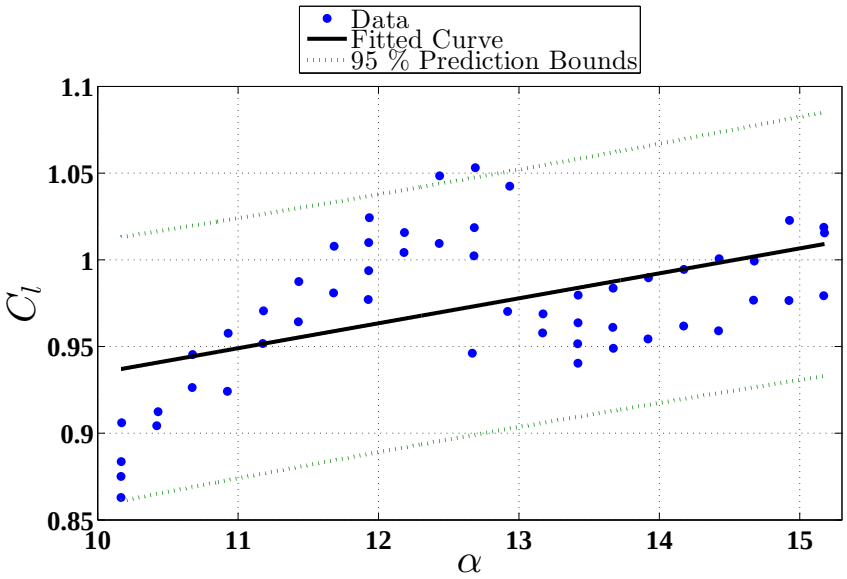

Figure 4.9: Linear fit of lift curve

		95% confidence bounds
K_0	0.7907	(0.7046, 0.8768)
K_1	0.01439	(0.007632, 0.02116)

Table 4.15: Parameters

4.4.4.2 Drag Polar

SSE	0.1304
R-Squared	0.2402
RMSE	0.05159

Table 4.16: Goodness of fit

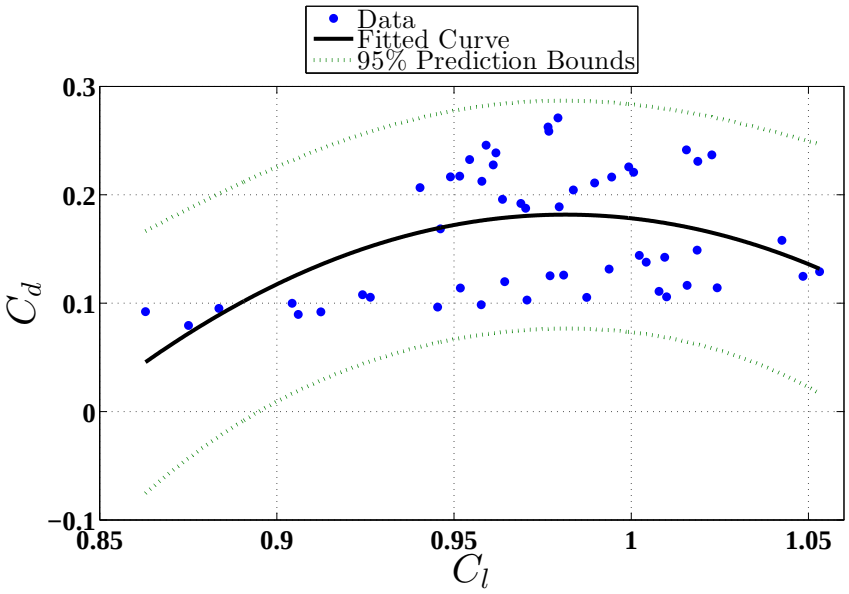

Figure 4.10: Quadratic fit of drag polar and residuals

		95% confidence bounds
K_0	-9.163	(-14.69, -3.634)
K_1	19.04	(7.543, 30.55)
K_2	-9.703	(-15.68, -3.728)

Table 4.17: Parameters

4.5 Region I Simulation Comparison

As discussed earlier FASER has a symmetric airfoil and therefore assuming potential flow will yield zero lift at zero α. Therefore in this region the results of the region will also be compared with the linear region parameters of the wind tunnel. This will allow direct comparison of the zero lift and zero lift drag parameters.

4.5.1 Lift Curve

The goodness of fits for this region is excellent. The lift curves produced by the simulation methods are highly linear. The goodness of fit metrics are presented in Table 4.18, the fits in Figure 4.11, and the estimated parameters in Table 4.20.

	SSE	R-Squared	RMSE
Wind Tunnel Linear Region	0.01283	0.9988	0.01416
Wind Tunnel Region I	0.001307	0.9965	0.009661
DATCOM	9.786e-06	0.9998	0.001043
Vortex Lattice	2.701e-07	1	0.0001732
Vortex Lattice Viscous	2.701e-07	1	0.0001732

Table 4.18: Goodness of fits for lift curves of Region I

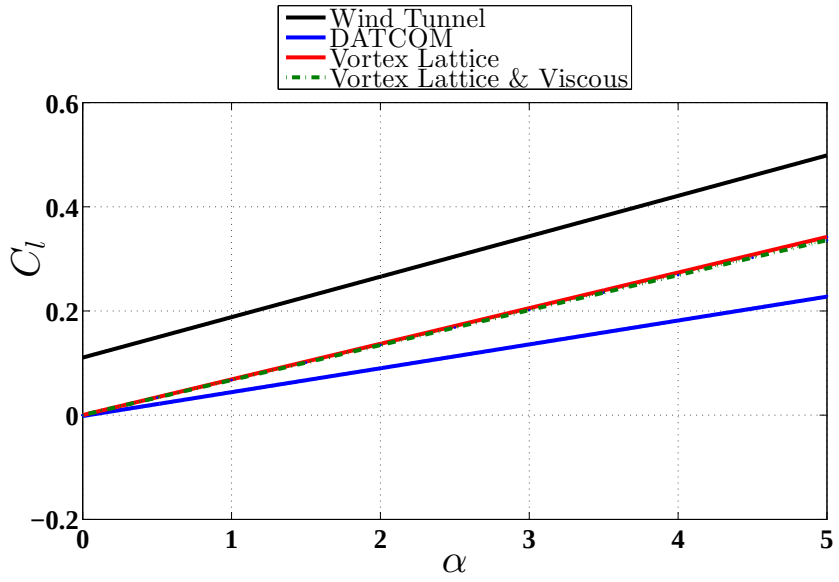

Figure 4.11: This is a plot of the simulation results, their linear fits, and 95% confidence bounds for Region I. The wind tunnel fit is also plotted for visual comparison.

	K_0	Δ_{K_0}	K_1	Δ_{K_1}
Wind Tunnel Linear Region	0.1134		0.0762	
DATCOM	-0.001682	1.0148	0.04584	0.3984
Vortex Lattice	0.0002203	0.9981	0.06713	0.1190
Vortex Lattice Viscous	0.0002203	0.9981	0.06713	0.1190

Table 4.19: Lift Curve Parameters comparison with the linear region of the wind tunnel data.

	K_0	Δ_{K_0}	K_1	Δ_{K_1}
Wind Tunnel Region I	0.1105		0.07762	
DATCOM	-0.001682	1.0152	0.04584	0.4094
Vortex Lattice	0.0002203	0.9980	0.06713	0.1351
Vortex Lattice Viscous	0.0002203	0.9980	0.06713	0.1351

Table 4.20: Lift Curve Parameters for Region I.

Vortex lattice is able to predict a lift slope value with a residual of only $K_1 = 0.1190$ when compared to the linear region. This can be seen by the parallel nature of the curves in Figure 4.11. So the curve is just a shift by the zero α error. Both simulation methods are unable to accurately calculate C_{l0} this is because both are working under the zero lift assumption of symmetric airfoils. DATCOM is the only method attempting to predict the body lift which would allow its calculation of C_{l0} to be shifted up from zero. So it is surprising that this method produces similarly bad results for C_{l0}. The Reynolds number of the test is $\approx 200,000$ which is the same order of magnitude as the limit of DATCOM. It is supposed that the DATCOM correction tables are too far away from the size of FASER to be accurately interpolated to.

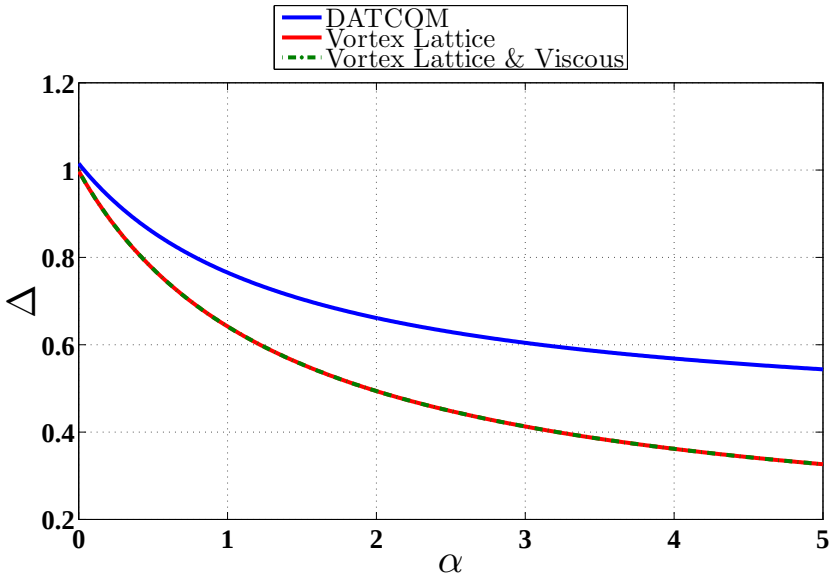

Figure 4.12: Residuals of linear fits are plotted verses α for the lift curves of Region I.

These short comings can be seen in the residual plot of Figure 4.12. The calculation of $K_0 \approx 0$ leads to a residual of 1. Then as the angle of attack is increased the residual will decrease. This is because the residual of the parameters is less than 1. Vortex lattice is seen to decrease faster because it has a better prediction than DATCOM. But both remain inaccurate and the residual plots will not flatten out.

4.5.2 Drag Polar

The goodness of fits for the drag polar in this region are excellent. The simulations are producing estimates of the drag polar that conforms well to the assumed form.

	SSE	R-Squared	RMSE
Wind Tunnel Linear Region	0.01283	0.9988	0.01416
Wind Tunnel Region I	0.0001122	0.6968	0.002938
DATCOM	6.269e-08	0.9991	8.852e-05
Vortex Lattice	4.125e-13	1	2.271e-07
Vortex Lattice Viscous	1.714e-09	1	1.464e-05

Table 4.21: Goodness of fits for drag polars of Region I.

In the case of the drag polar the fits are not only suffering from a miscalculation of C_{l0} but also from an underestimation of C_{d0}. This leads to the shift seen in Figure 4.13. Specifically the shift can be seen in comparing the Linear region plot where the location of the beginning of the curve is shifted up by its by the miscalculation of C_{d0} when compared to the simulations. We can see that the plot of the wind tunnel fit for Region I is much higher than the others, again this is because the zero lift point of FASER is not at zero α as predicted by potential flow methods. DATCOM is able to produce the closest estimate as it is attempting to take into account the body drag as well as viscous forces. It is interesting that the vortex lattice code including viscous forces produces a similar K_0 result as DATCOM. This could arise from the fact that at zero α the largest contribution to viscous drag will be the whetted area of the wing and tail plane. Which lines up with what was expected in the discussion of the wind tunnel results. Because the simulations under calculate the lifting performance the drag will also be under estimated.

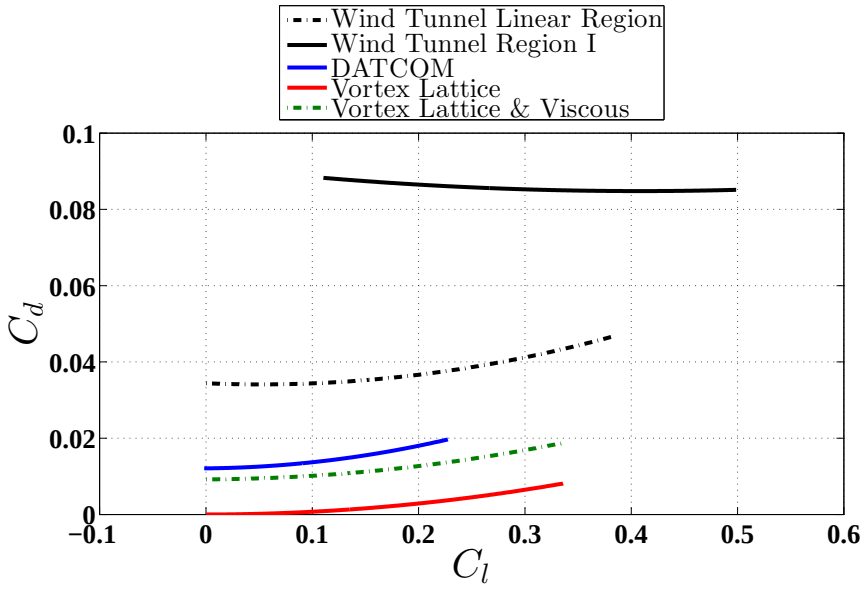

Figure 4.13: This is a plot of the simulation results, their quadratic fits, and 95% confidence bounds for Region I. The wind tunnel fit is also plotted for visual comparison.

	K_0	Δ_{K_0}	K_1	Δ_{K_1}	K_2	Δ_{K_2}
Wind Tunnel Linear Region	0.0372		-0.0376		0.1143	
DATCOM	0.0121	0.6747	0.002355	1.0626	0.1361	-0.1907
Vortex Lattice	2.635e-07	1.0000	-1.066e-05	0.9997	0.07204	0.3697
Vortex Lattice Viscous	0.009208	0.7525	0.001235	1.0328	0.08116	0.2899

Table 4.22: Drag Polar Parameters and their corresponding residual comparison of Region I of the simulations to the linear region of the wind tunnel.

An interesting result from Table 4.22 is the simulations are able to calculate the induced drag more accurately than the form drag. This is as expected from the preceding discussion, but what is interesting is the simulation models do not calculate a term proportional to C_l well. The wind tunnel data conforms well to the three parameter model of Equation 4.7 while the simulations would be better fit by a two term model. This is assumed to be an inerrant trait of how the codes separate the total drag contribution of induced drag and form drag.

	K_0	Δ_{K_0}	K_1	Δ_{K_1}	K_2	Δ_{K_2}
Wind Tunnel Region I	0.09132		-0.03197		0.03918	
DATCOM	0.0121	0.8675	0.002355	1.0737	0.1361	-2.4737
Vortex Lattice	2.635e-07	1.0000	-1.066e-05	0.9997	0.07204	-0.8387
Vortex Lattice Viscous	0.009208	0.8992	0.001235	1.0386	0.08116	-1.0715

Table 4.23: Drag Polar Parameters and their corresponding residual for Region I.

The residual plot for the Linear Region comparison to Region I can be seen in Figure 4.14. The shape of the residual plot comes from the fact that C_d is dependent on the square of C_l which flips the concavity of the residual plot. The plot will start at the initial residual of K_0 but in the case of

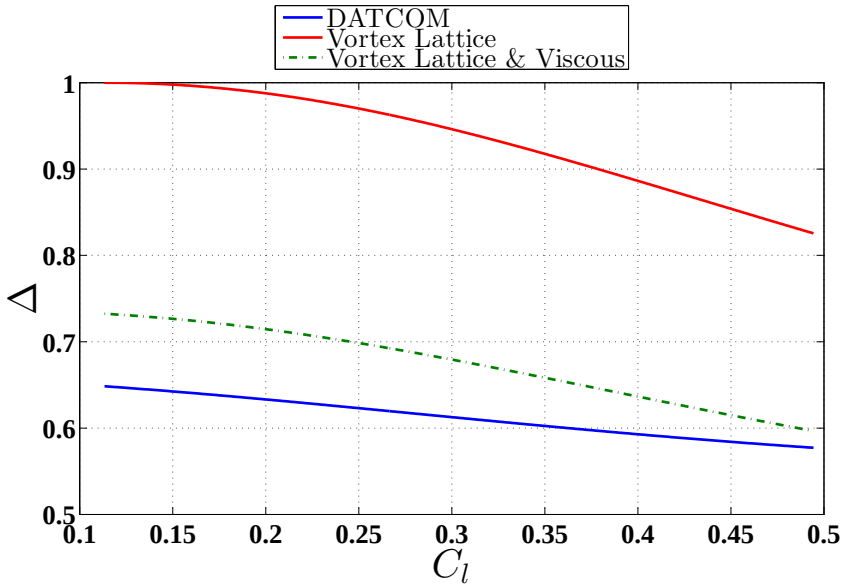

Figure 4.14: Residuals of quadratic fits plotted at the C_l values of the wind tunnel data for Region I.

The miscalculation of C_{l0} can be removed by plotting the residual of fitted simulation equations over the range of C_l of the wind tunnel data. The residual plot can be seen in Figure 4.15. The shape of the residual plot comes from the fact that C_d is dependent on the square of C_l which flips the concavity of the residual plot. But for again the estimates of the parameters are too far off in order to have the residual plot

flatten out. At the minimum location of the wind tunnel data the best fit, DATCOM, has a residual of ≈ 0.6 and is dropping as the effect of the miscalculation of K_2 begins to dominate. Also the plot starts at 1 which is captured in the value of Δ_{K_0} for the methods. This says the calculation of C_{d0} is very poor.

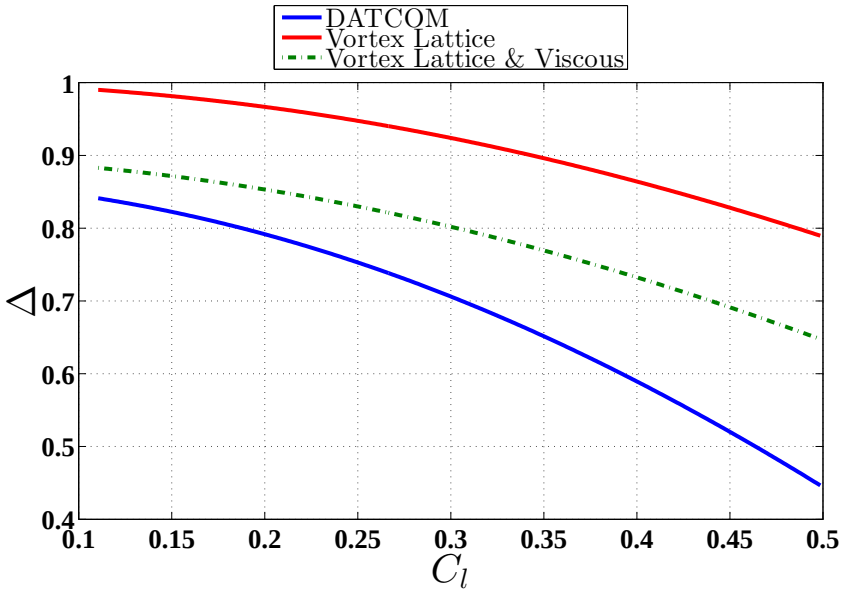

Figure 4.15: Residuals of quadratic fits plotted at the C_l values of the wind tunnel data for Region I.

4.6 Region II Comparison

4.6.1 Lift Curve

	SSE	R-Squared	RMSE
Wind Tunnel	0.005202	0.9889	0.01472
DATCOM	2.694e-06	1	0.0003868
Vortex Lattice	3.583e-06	1	0.0004462
Vortex Lattice Viscous	3.583e-06	1	0.0004462

Table 4.24: Goodness of fits for lift curves of Region II

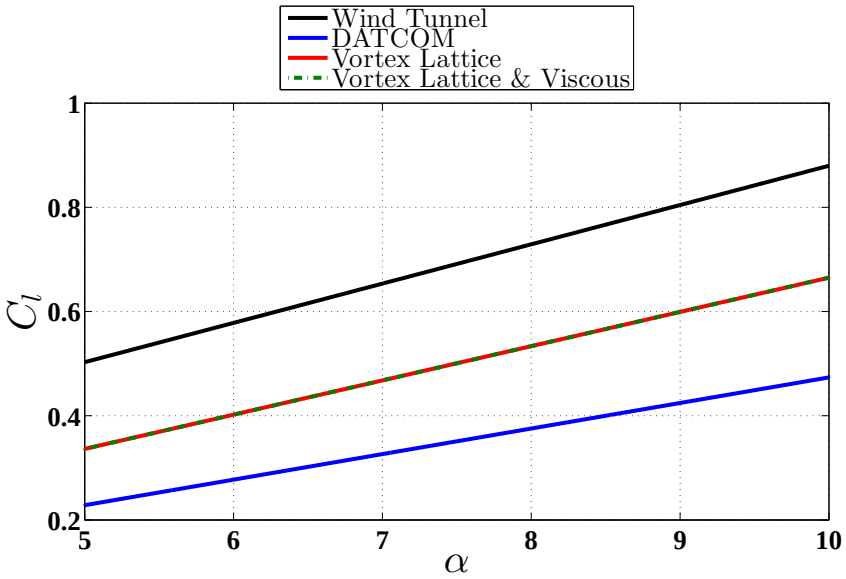

Figure 4.16: This is a plot of the simulation results, their linear fits, and 95% confidence bounds for Region II. The wind tunnel fit is also plotted for visual comparison.

	K_0	Δ_{K_0}	K_1	Δ_{K_1}
Wind Tunnel	0.1257		0.07541	
DATCOM	-0.01703	1.1195	0.04906	0.3494
Vortex Lattice	0.007591	0.9396	0.06574	0.1282
Vortex Lattice Viscous	0.007591	0.9396	0.06574	0.1282

Table 4.25: Lift Curve Parameters for Region II.

The lift slope prediction of vortex lattice in this region has the best residual yet as seen in Table 4.25. In this region the effect of the zero lift condition of the symmetric airfoil is less present. Also the effect of body lift and other sources is heavily outweighed by the lift produced by the lifting surfaces. The assumptions made in the vortex lattice code again produce much better results for this small aircraft than DATCOM.

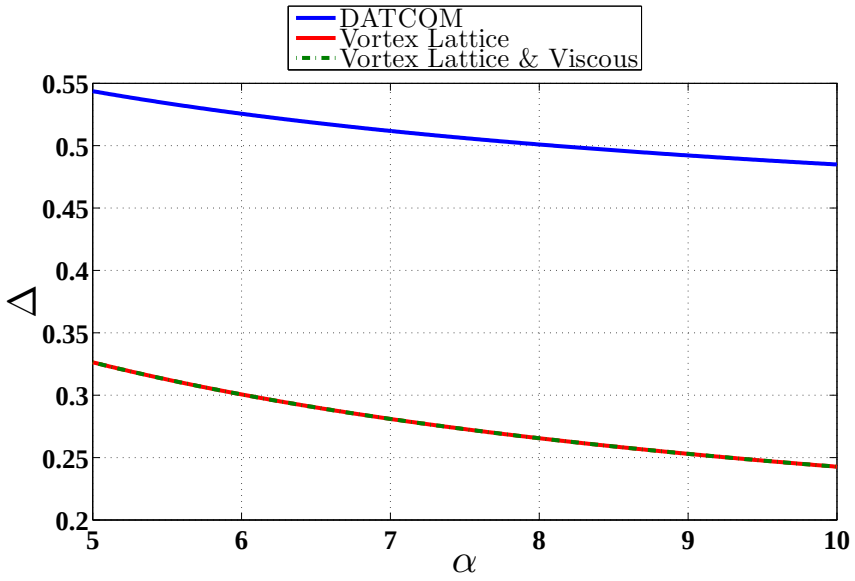

Figure 4.17: Residuals of linear fits are plotted verses α for the lift curves of Region II.

The effect of a more accurate prediction of the lift slope can be seen in the flattening of the residual plot, Figure 4.17. As the angle of attack increased this parameter dominates and outweighs the zero lift.

4.6.2 Drag Polar

	SSE	R-Squared	RMSE
Wind Tunnel	.0003037	0.9519	0.003634
DATCOM	3.345e-09	1	1.403e-05
Vortex Lattice	5.031e-12	1	5.44e-07
Vortex Lattice Viscous	1.099e-07	0.9999	8.04e-05

Table 4.26: Goodness of fits for drag polars of Region II.

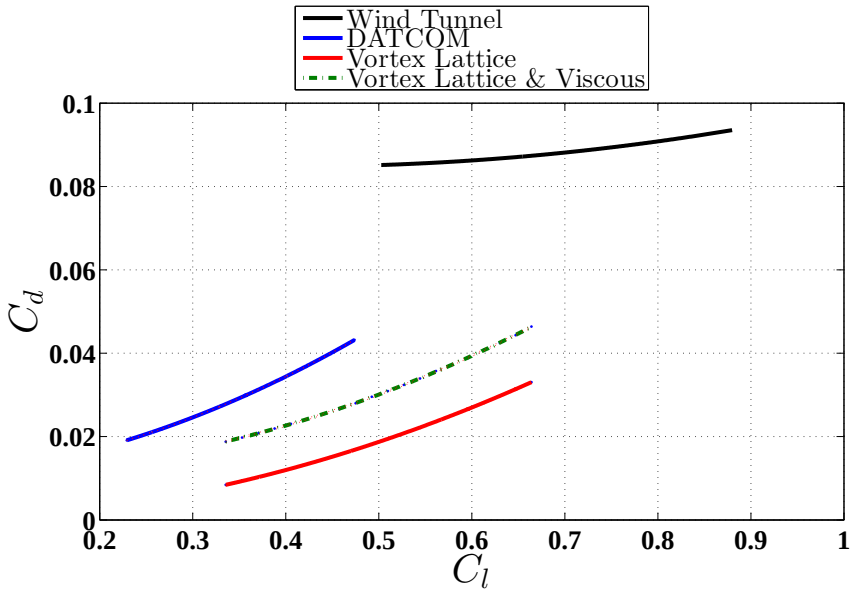

Figure 4.18: This is a plot of the simulation results, their quadratic fits, and 95% confidence bounds for Region I. The wind tunnel fit is also plotted for visual comparison.

	K_0	Δ_{K_0}	K_1	Δ_{K_1}	K_2	Δ_{K_2}
Wind Tunnel	0.05354		0.03842		0.05354	
DATCOM	0.009631	0.8201	0.01384	0.6398	0.1202	-0.5159
Vortex Lattice	6.083e-05	0.9989	-0.000346	1.0090	0.07532	-0.4068
Vortex Lattice Viscous	0.0114	0.7871	-0.00897	1.2335	0.09267	-0.7309

Table 4.27: Drag Polar Parameters and their corresponding residual for Region II.

The codes are again over predicting the dynamic coefficient K_2 and under predicting the static coefficient K_0. Comparing back to the wind tunnel discussion of the elliptical lift idealization the codes are predicting even beyond this measure.

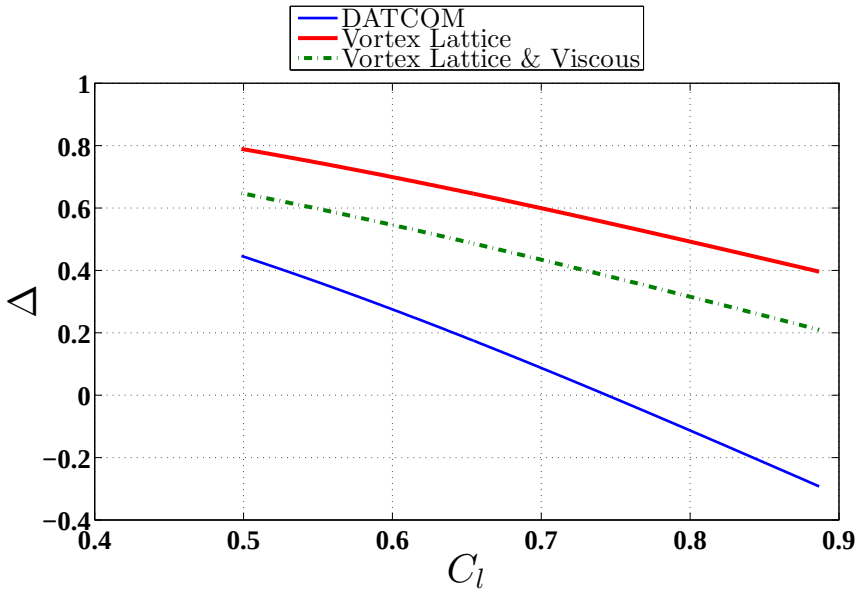

Figure 4.19: Residuals of quadratic fits plotted at the C_l values of the wind tunnel data for Region II.

4.7 Region III Comparison

The results of Region III are provided below for completeness. As stated prior the aircraft has entered the stall region here and the codes do not predict stall. Thus the comparison in this region is meaningless.

4.7.1 Lift Curve

	SSE	R-Squared	RMSE
Wind Tunnel	0.005202	0.9889	0.01472
DATCOM	0.0001587	0.998	0.002969
Vortex Lattice	9.27e-06	0.9999	0.0007176
Vortex Lattice Viscous	3.583e-06	1	0.0004462

Table 4.28: Goodness of fits for lift curves of Region III.

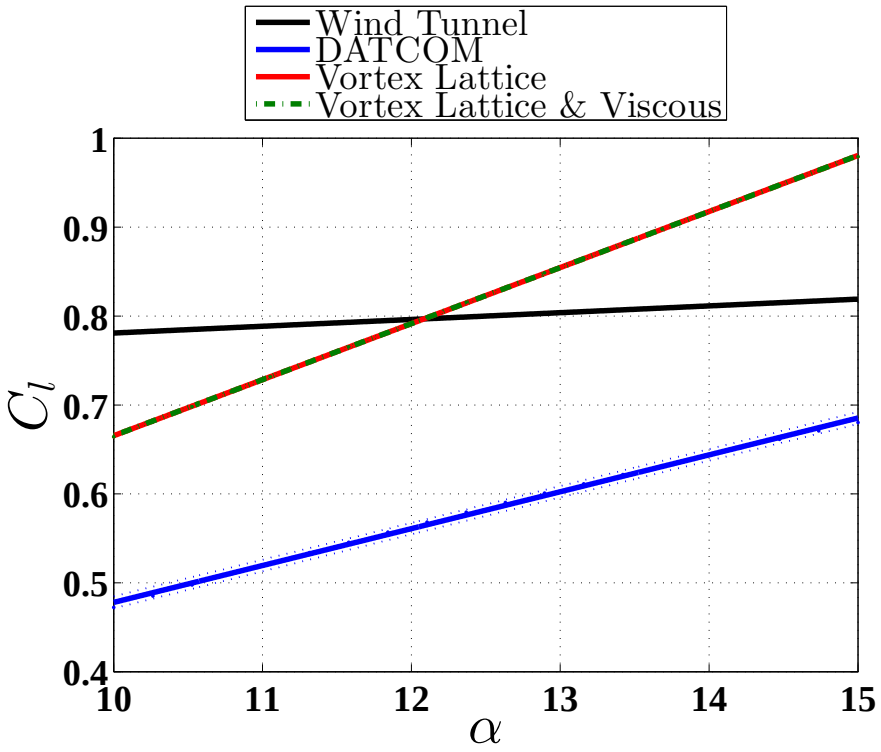

Figure 4.20: This is a plot of the simulation results, their linear fits, and 95% confidence bounds for Region III. The wind tunnel fit is also plotted for visual comparison.

	K_0	Δ_{K_0}	K_1	Δ_{K_1}
Wind Tunnel	0.7907		0.01439	
DATCOM	0.06311	0.9202	0.04148	-1.8826
Vortex Lattice	0.03498	0.9558	0.06305	-3.3815
Vortex Lattice Viscous	0.03498	0.9558	0.06305	-3.3815

Table 4.29: Lift Curve Parameters for Region III.

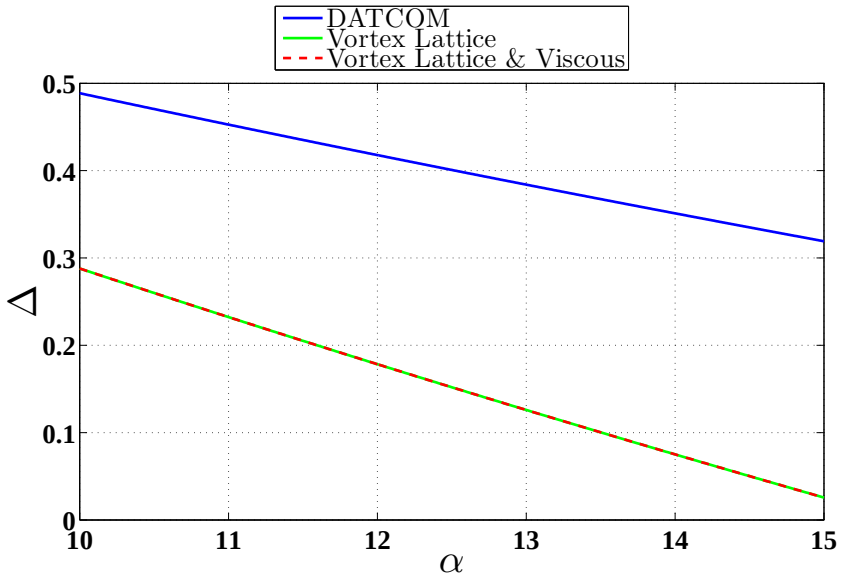

Figure 4.21: Residuals of linear fits are plotted verses α for the lift curves of Region III.

4.7.2 Drag Polar

	SSE	R-Squared	RMSE
Wind Tunnel	0.1304	0.2402	0.05159
DATCOM	1.902e-09	1	1.058e-05
Vortex Lattice	3.626e-12	1	4.618e-07
Vortex Lattice Viscous	1.899e-07	0.9999	0.0001057

Table 4.30: Goodness of fits for drag polars of Region III.

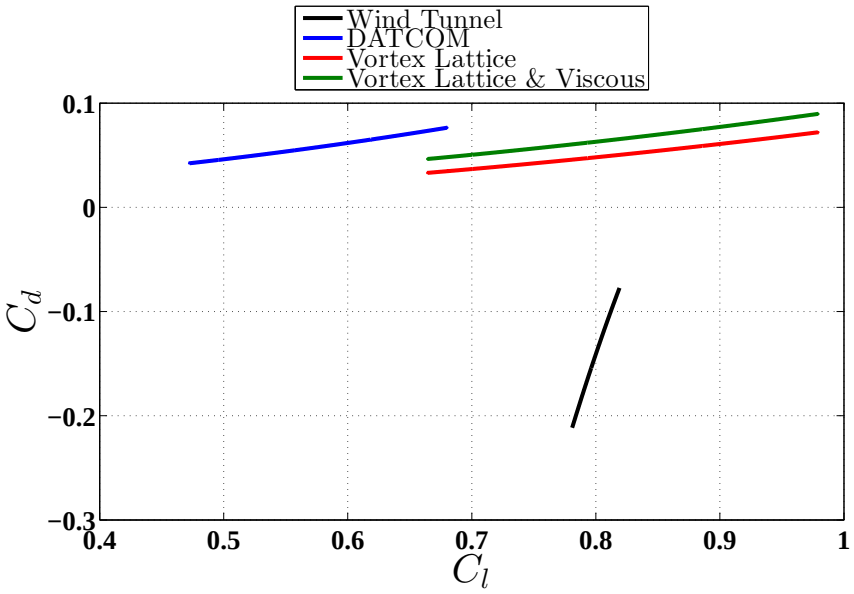

Figure 4.22: This is a plot of the simulation results, their quadratic fits, and 95% confidence bounds for Region III. The wind tunnel fit is also plotted for visual comparison.

	K_0	Δ_{K_0}	K_1	Δ_{K_1}	K_2	Δ_{K_2}
Wind Tunnel	-9.163		19.04		-9.703	
DATCOM	0.01046	1.0011	4e-06	1.0000	0.1425	1.0147
Vortex Lattice	0.0003551	1.0000	-0.00123	1.0001	0.07599	1.0078
Vortex Lattice Viscous	0.01218	1.0013	-0.006866	1.0004	0.08785	1.0091

Table 4.31: Drag Polar Parameters and their corresponding residual for Region III.

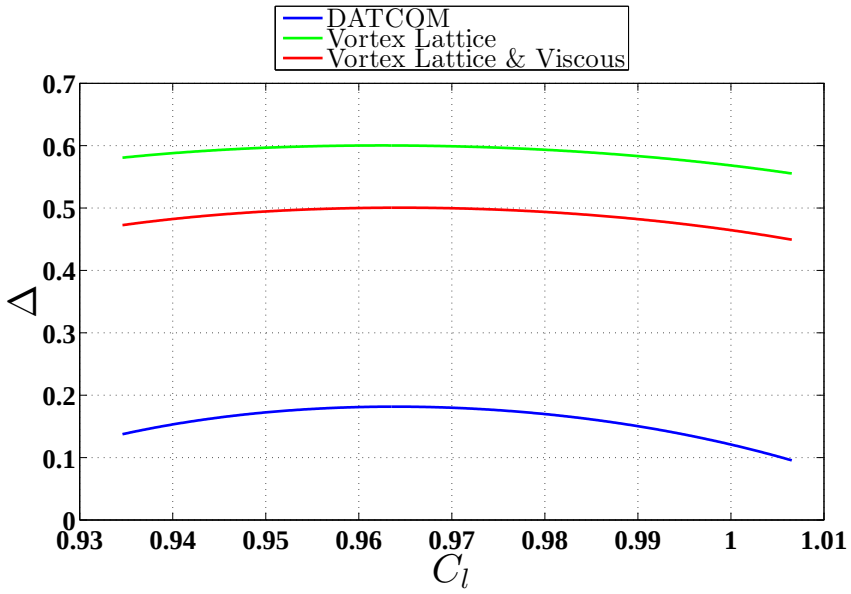

Figure 4.23: Residuals of quadratic fits plotted at the C_l values of the wind tunnel data for Region III.

Chapter 5

Conclusion

In this chapter we will provide concluding remarks and suggestion for future work.

5.1 Summary of Findings

Great interest in the small UAV has risen the recent years. This is because of many factors but a large part is due to their cost and ease of use. Because of the recent rise in interest there is a rising demand for tools to design this class of aircraft. But it is not clear if the tools developed over the century of manned flight are appropriate to use for this class of aircraft.

Because of the low cost nature of UAVs two low cost tools where chosen as candidates to be used in the prediction of performance. These two were DATCOM and Vortex Lattice and an open source wrapper CEASIOM was used to more easily utilize these tools. The FASER airframe was chosen to be used as the comparison as accurate wind tunnel data is available for it. The predictions of the software could then be compared to the wind tunnel data for validation.

From the results of the validation study it was shown that these two tools may not be completely appropriate for the task. The methods are able to predict the "dynamic" parameters with some accuracy but the static parameters are poorly calculated. Many reasons were discussed but one main reason for each method stands out. For DATCOM the empirical look up tables do not extend low enough into the Reynolds number range considered. And because aerodynamic effects through the

Reynolds number range do not scale linearly the empirical corrections do not capture the true aerodynamics of FASER. For vortex lattice the potential flow assumptions are not completely valid at this size of vehicle. Many non-linear aerodynamic effects are magnified at this scale and violate the assumptions.

5.2 Suggested Future Research

There could be promise in providing DATCOM with empirical tables of UAVs and testing to see if the semi-empirical methods come closed to the true dynamics. Also there has been recent advances in extending vortex lattice and its potential flow assumptions to be valid at this scale. All of this might not be worth the effort as CFD advances and becomes more user friendly and less expertise and experience is needed to run.

Bibliography

[1] Raymer, D. P., *Enhancing Aircraft Conceptual Design Using Multidisciplinary Optimization*, Ph.D. thesis, Department of Aeronautics, Royal Institute of Technology (KTH), 2002.

[2] JamesonA, O., "Relative roles of computational fluid dynamics and wind tunnel testing in the development of aircraft," *CURRENT SCIENCE*.

[3] JamesonA, O., "50 Years of Transonic Aircraft Design," *Prog Aerospace Sci*.

[4] Roskam, D. J., *Airplane Design, Part VI: Preliminary Calculation of Aerodynamic, Thrust, and Power Characteristics*, DARcorporation, 1st ed., 2000.

[5] Company, M. D. A., "USAF Stability and Control DATCOM," Air Force Flight Dynamics Laboratory Technical Report 793032, 1979.

[6] D. B. Owens, D. E. Cox, E. A. M., "Development of a low-cost sub-scale aircraft for ight research: The FASER project," *25th AIAA Aerodynamic Measurement Technology and Ground Testing Conference (2006-3306)*.

[7] Owens, D. B. Aubuchon, V., "FASER Static Test 153 NASA LaRC," `http://purl.umn.edu/119574`.

[8] Kuethe, A. M., *Foundations of Aerodynamics*, John Wiley Sons, New York, 5th ed., 1998.

[9] Melin, T., *A Vortex Lattice MATLAB Implementation for Linear Aerodynamic Wing Application*, Master's thesis, Royal Institute of Technology (KTH), 2000.

[10] R. von Kaenel, A. Rizzi, J. O. e. a., "CEASIOM: Simulating Stability Control with CFD and CSM in Aircraft Conceptual Design." *26th International Congress of the Aeronautical Sciences, ICASL*, 2008.